EXPERIMENTAL CONSTRUCTION AND ANALYSIS OF A PASSIVE LASER RING RESONATOR

By

TAUFIQ HABIB

Bachelor of Science

N.E.D. University

Karachi, Pakistan

1983

Submitted to the Faculty of the
Graduate College of the
Oklahoma State University
in partial fulfillment of
the requirements for
the Degree of
MASTER OF SCIENCE
December, 1986

EXPERIMENTAL CONSTRUCTION AND ANALYSIS

OF A PASSIVE LASER RING

RESONATOR

Thesis Approved:

J. R. Bigler

Thesis Adviser

Richard L. Cummins

N. V. V. J. Swamy

Bennett Brown

Norman N. Durham

Dean of the Graduate College

PREFACE

This study was conducted to learn more about ring resonators and problems associated with actually building one in the laboratory. The single-beam model constructed revealed many sources of error, some of which became evident only after observing the behavior of the ring. A study of the erratic output indicated that certain precautions were necessary in order to build a sensitive resonator. The major application of ring resonators is in the field of ring laser gyroscopes which can be made into very sensitive rotation measuring devices.

My interest in this field was initiated by my committee chairman, Dr. Bilger, who has always been more than ready to provide valuable assistance, and has done the majority of the work in proofreading this manuscript. I would like to individually thank each of my committee members; Dr. Basore, Dr. Cummins, Dr. Ramakumar, and Dr. Swamy, for their time and effort in reading the rough draft of this thesis and providing me with valuable suggestions for further improvement. In addition, I would like to thank Dr. Cummins for the loan of his personal computer which made much of my data acquisition and analysis possible.

The department chairman, Dr Baker, has been extremely kind in providing me with some of the equipment I needed for the construction of the ring, and has always been more than willing to help.

Much knowledge has been gleaned from my working on a project like this; there are many possibilities in this kind of undertaking, and I would like to welcome any future student willing to explore more in this field.

TABLE OF CONTENTS

LIST OF TABLES

LIST OF FIGURES

LIST OF SYMBOLS

a_f	output amplitude
a_i	input amplitude
α	tilt error
δ	offset error
d	phase delay
Δ_z	small translation along optical axis
Δ_ϕ	small tilt in plane of optical axis
ε	offset error (in misalignment parameter only)
F	finesse
f	focal length
FSR	Free Spectral Range
λ	(Lambda) wavelength
$\square$	mismatch parameter
P_o, P_L	power content of source
Q	quality factor
q	complex Gaussian parameter
q	longitudinal value of a TEM mode
R	reflectivity (power)
R	radius of curvature
r	reflectivity (amplitude)
S	length
S(x,y)	power density at a point on a cross-sectional z-plane

T	transmittivity (power)
t	transmittivity (amplitude)
θ	incident angle
θ	(theta) angle in a spherical coordinate system
Φ	(phi) angle in a spherical coordinate system
um	micrometer
μ	m or n (qualifiers for axial mode type)
v	x or y
ω	wave frequency
w	spot size
w_a	major axis length
w_o	waist size
w_{OL}	source waist size
w_{OR}	ring waist size
ξ	misalignment parameter
ξ	dummy variable
z_w	Rayleigh length

CHAPTER I

INTRODUCTION

Background

Optical ring cavities have been in use since Oliver Lodge constructed one in 1897 (Heer, 1984) to measure the "drag of ether". Since then, the main use of these cavities has been to study rotational effects or to measure the drag of light in the presence of a medium (Stowell, 1974). According to current literature, the first resonant ring cavity was proposed by Rosenthal (1962) in which two counter-propagating laser beams were generated by use of an active medium contained in the resonator. Since then the active ring laser gyroscope has matured into a sophisticated device used nowadays by aircraft for navigation.

The first passive ring laser resonator was proposed by Ezekiel (1977) in which an external laser was used to inject the two beams. The passive ring laser resonator has some advantages as well as disadvantages over the active type of device, and has been a constant source of study since its invention. Of particular interest are the errors introduced by misinjection of the source (Sayeh, 1985), and by internal mirror tilts and shifts (Stedman, 1986).

Ezekiel (1978) observed the existence of higher-order modes due to misalignment (both internal & external).

A passive ring resonator can support a large number of different modes unlike an active resonator which only resonates in modes having sufficient loop-gain. Alignment is therefore an important factor in the construction of passive resonant cavities. It is possible to predict alignment errors of a passive ring laser gyroscope (PRLG) by studying errors associated with a cavity which has only one resonant beam instead of two counter-propagating beams, since errors would affect both beams in the same way.

Objectives and Order of Presentation

The main purpose behind this study is to quantitatively assess certain parameters related to the building of a successful passive ring resonator. Figure 1 shows the associated errors in block diagram form.

A complete study of the source laser needs to be done, and chapter two is devoted to this. Length, position, and tilt of the optical axis must be measured, and eigenmodes of the ring need to be calculated. Resonator finesse (definition, see Appendix A) needs to be calculated after a study of mirror reflectivities.

The source must be aligned and matched with the ring to achieve proper resonance. The effect of residual errors may then be investigated. Misalignment has been observed to produce Hermite-Gaussian modes in the output of the

resonator, and these are the most commonly observed higher-order modes in a laser resonator.

Due to a lack of a formal theory at present, computer simulation will be used to determine the effect of mirror movements .

The final setup to be achieved is shown in Figure 2.

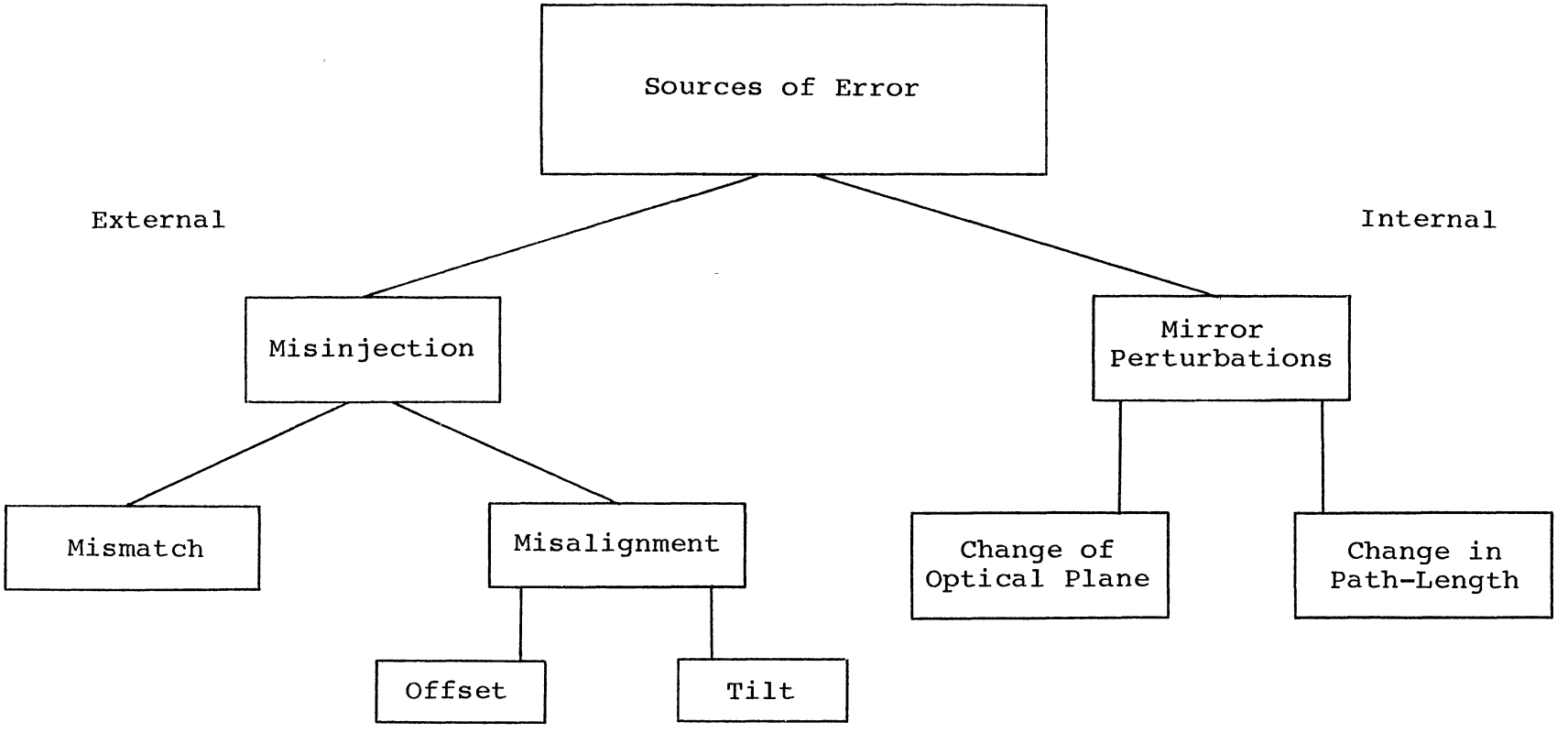

Figure 1. Types of destabilizing errors expected in a passive ring resonator.

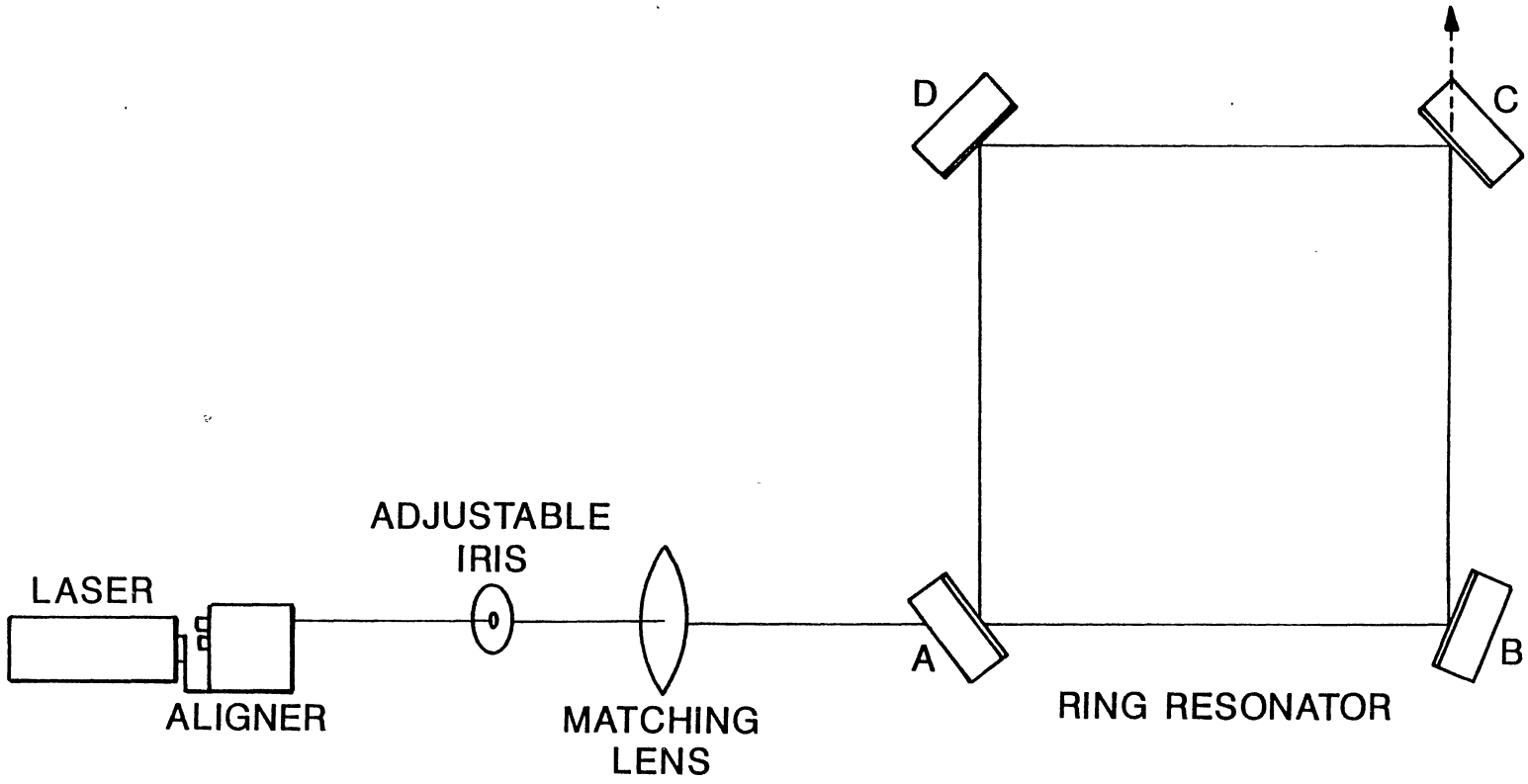

Figure 2. The final setup used in this study

CHAPTER II

PARAMETERS OF THE INJECTION LASER

Introduction

The source used was a frequency-stabilized single frequency HeNe laser. The laser head has connected to it a power supply cord and a cable for feedback/control which keeps the output of the laser to a single longitudinal mode of constant frequency (see specifications, next page) by thermally controlling the laser cavity length. The error signal for the heater control is provided by the intensity difference between two different internal longitudinal modes on the gain curve (see Figure 3). The voltage supply to the heater in the laser-head is controlled so as to keep this difference as small as possible and this has the effect of fixing the two modes in the frequency domain since their spacing is constant and equal to the free spectral range, c/2L (L is the length of the laser cavity).

Only one of the modes is allowed to escape and forms the output of the laser.

The parameters of the Coherent Model 200 laser as described in the operators manual are given on the next page.

Power Output, Po : Ø.86mW < Po < Ø.96mW

Mode extinction for 2nd and 3rd order modes : < Ø.1 %

Short-term frequency stability < $\pm$ 1 MHz drift in 15 min

Long-term frequency stability ~ 25 MHz

Free Spectral Range : 565 MHz

Beam 'contour' diameter ($1/e^2$ point) : Ø.6 mm ?

Full-angle beam divergence : 1.3 mrad

Amplitude noise (1Ø Hz - $1Ø^7$ Hz) : < Ø.2 % RMS

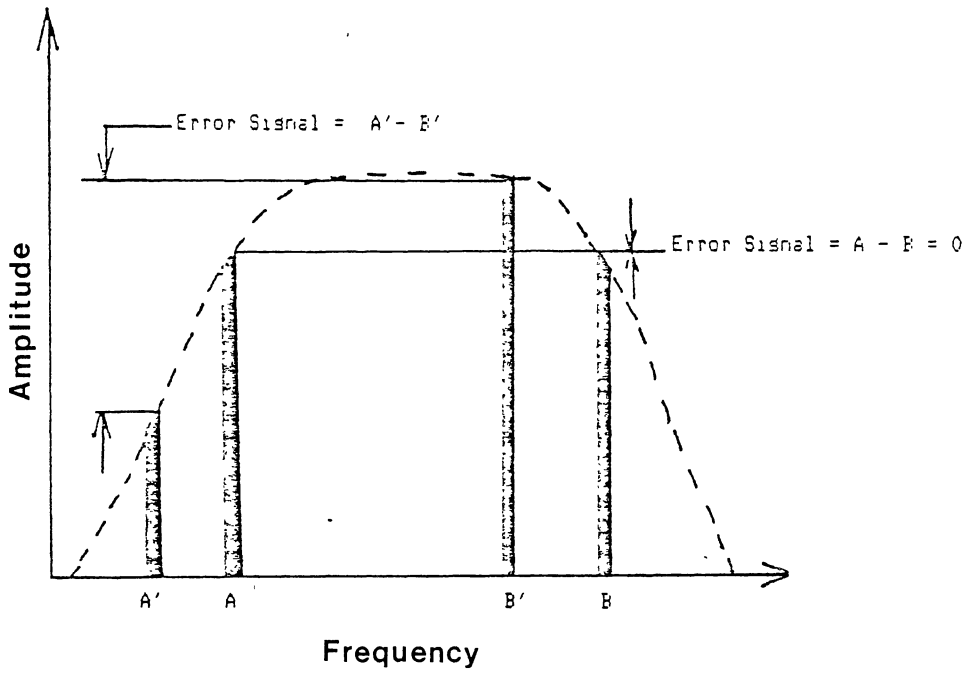

Figure 3. How error signals are produced by change in mode position; as the modes drift form A and B to A' and B', an error signal is produced, and is used to provide feedback for the laser. (Reproduced from the Coherent laser operator's manual).

Output Power Variation

A check on power fluctuations of the laser-beam was performed by placing a detector directly in the path of the beam, hooked up to a voltmeter and digitizer.

The detector output was monitored for over an hour and the results are displayed in the graph below. After stabilization, the RMS of the variation was estimated to be < Ø.5 %

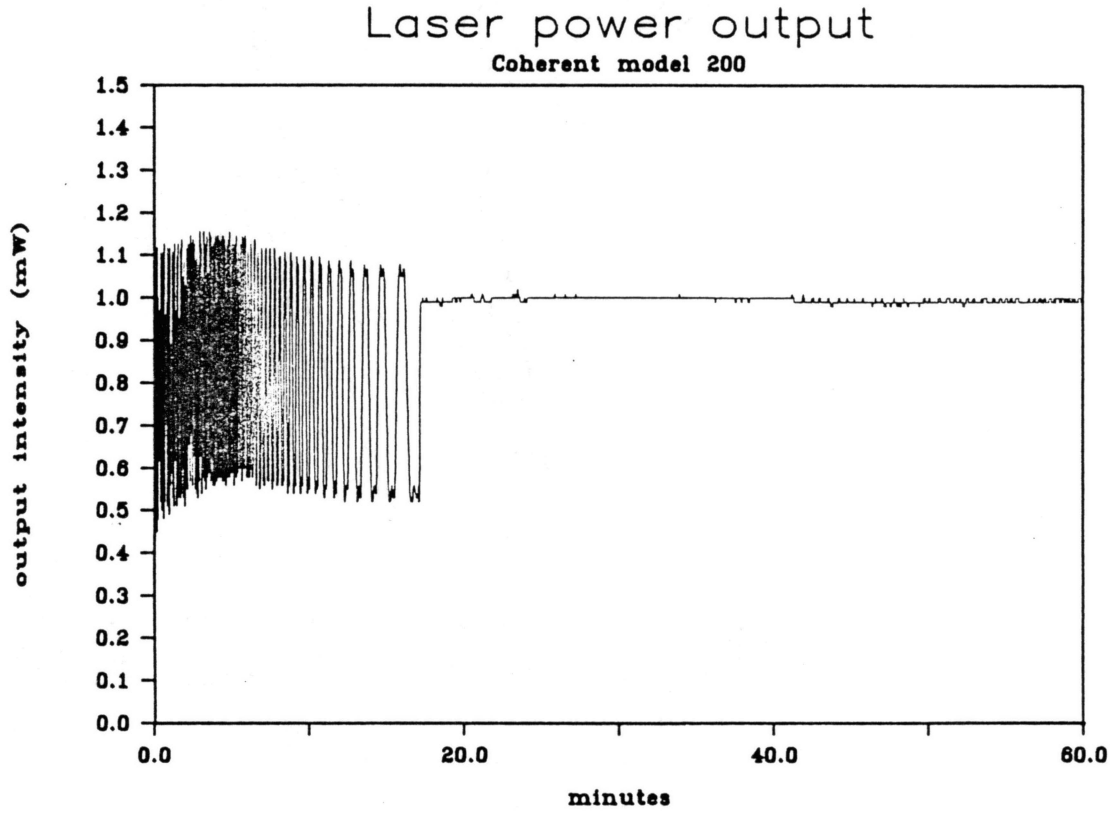

Figure 4. Power output of source vs time after power is switched on (Ø min). Note that the feedback-control system starts operating 2Ø min after power-on.

Beam Intensity Profile

Photographs of the laser output indicate a roughly Gaussian shape with a lot of extraneous radiation, some of which may be due to the frequency-stabilization optics inside the laser head. The photographs are displayed in Figure 6. Two tests were done to verify the Gaussian profile along a cross-section of the beam, and to determine if the beam was astigmatic.

For reference and consistency, a right-handed xyz coordinate system will be employed with the z-axis representing the forward direction of travel of the laser beam.

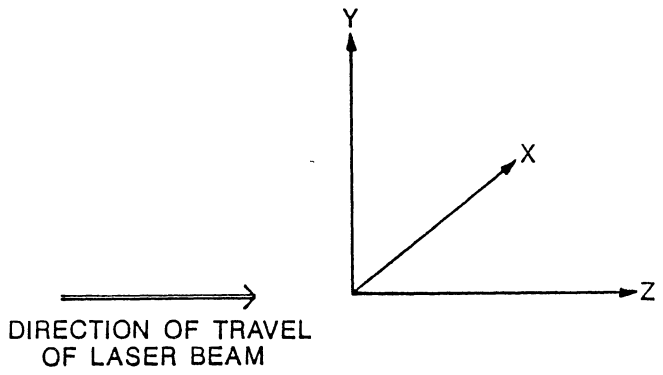

Figure 5. The reference coordinate system.

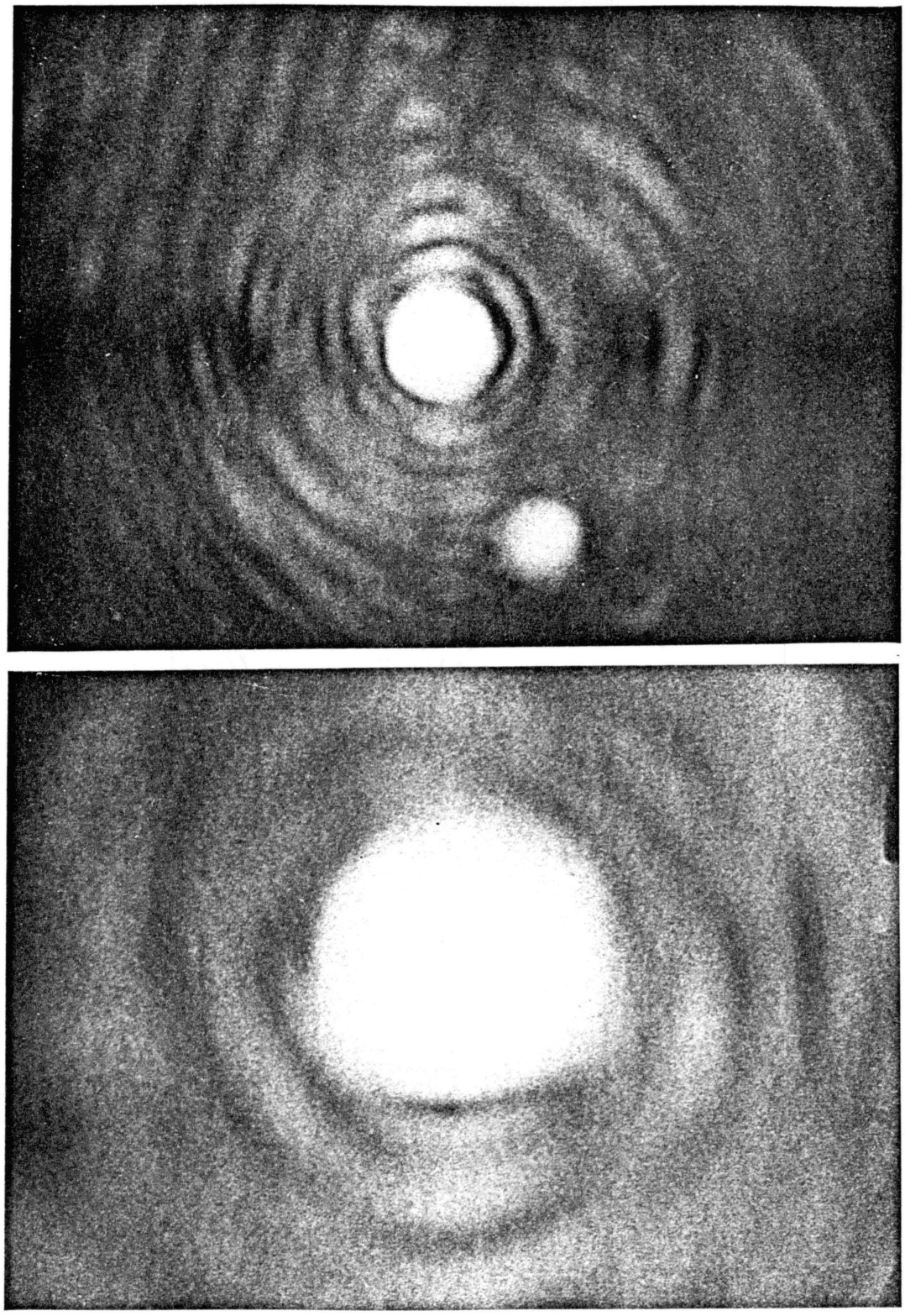

Figure 6. Photographs of the source laser; note the stray radiation around the main beam.

Gaussian Intensity Profile

The spot size and the Gaussian profile of a spatially filtered version of the beam were determined using knife-edge scanning techniques developed earlier in the laboratory [Bilger & Habib, 13].

The variation of power density along, say the x-axis on a cross-section of a Gaussian beam is given by:

$$S(x,y) = \frac{2}{\pi}\frac{Po}{w_x w_y}\exp\left[-2(x-x_o)^2 / w_x^2\right]\exp\left[-2(y-y_o)^2 / w_y^2\right] \quad (1)$$

where Po is the total power in the beam; $\frac{2}{\pi}\frac{Po}{w_x w_y}$ is the power density in the center, and x_o is the x-coordinate of the center of the beam.

The power spilling over a straight-edge intersecting the beam can be found by integrating S(x,y) over dx and dy, to give us the complementary error function. A plot of this function vs blade position is given by the solid curve in Figure 7.

A least-squares program on the ECEN VAX computer (a Bilger-Habib effort) can be used to fit the measured power ratios vs blade position using an approximation for the complementary error function to determine the spot size w . Measurements of power spilling over the edge vs blade position performed along a cross-section of the beam at a distance of 45 cm from the front end of the laser-head are represented by points on the curve in Figure 7 . Note that

the data fit very closely on a theoretical curve signifying a very nearly Gaussian beam.

The least-squares program gave the spot size as 444 $\pm$ 4 um, at a distance 47.5 cm from the laser waist.

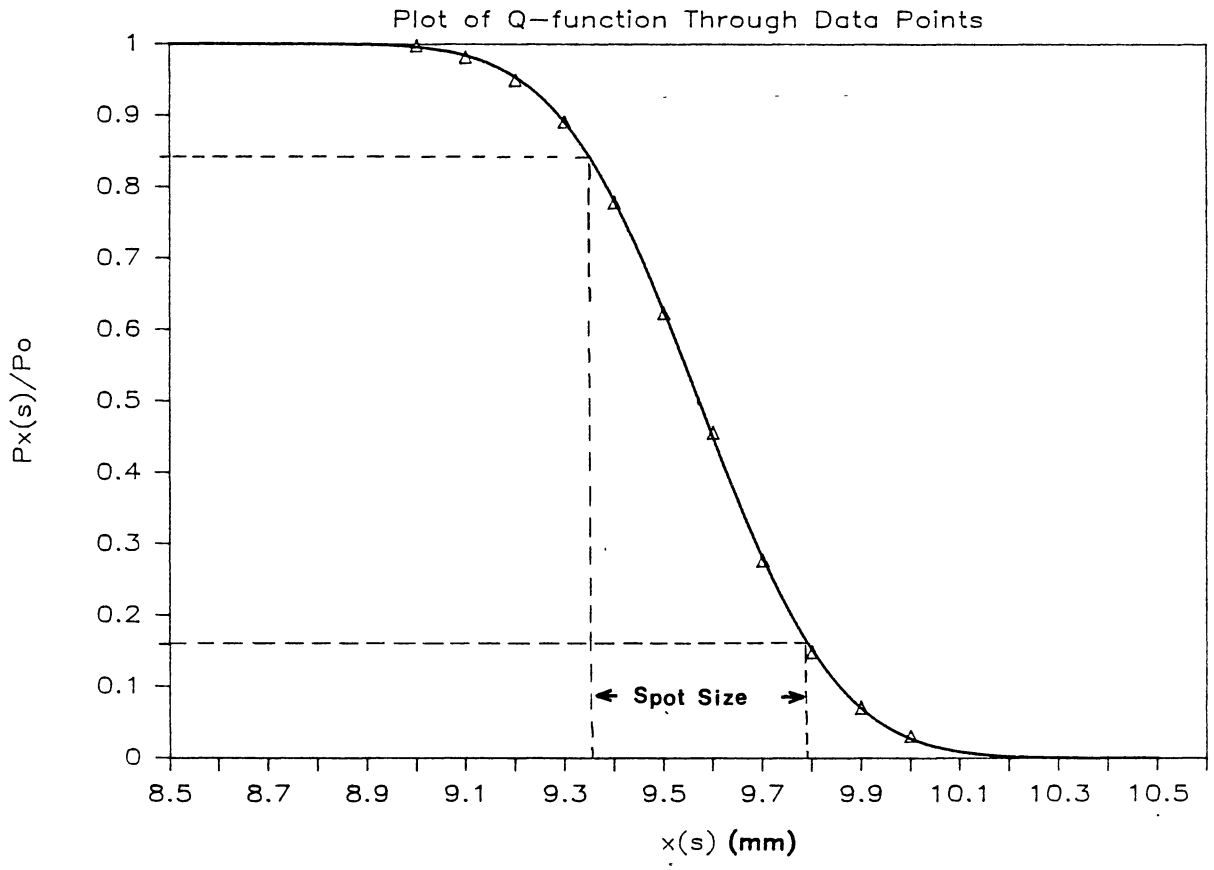

Figure 7. Result of a knife-edge scan of the source beam at an arbitrary angle, 45 cm from the laser. The spot size obtained is 444 $\pm$ 4 um.

Verification of astigmatism

Gaussian beams can be astigmatic i.e. have different spot sizes along the x and the y axes. Reverting again to the knife-edge scanning process, we determined a way to find the characteristics of an astigmatic Gaussian beam. This can be done by scanning along various angles in the xy-plane to find the spot size as a function of scanning angle.

A least-squares fit provides us with the values of the major axis w_a, the eccentricity e and the angle of tilt α of the major axis with the x-axis. A plot of measured values on an circle of radius 452 um shows a close fit.

The calculated values of the parameters are:

$w_a = 452 \pm 2$ um

$e = 0.17 \pm 0.1$

$\alpha = 90 \pm 42^{o}$

The output beam was found to be almost circular.

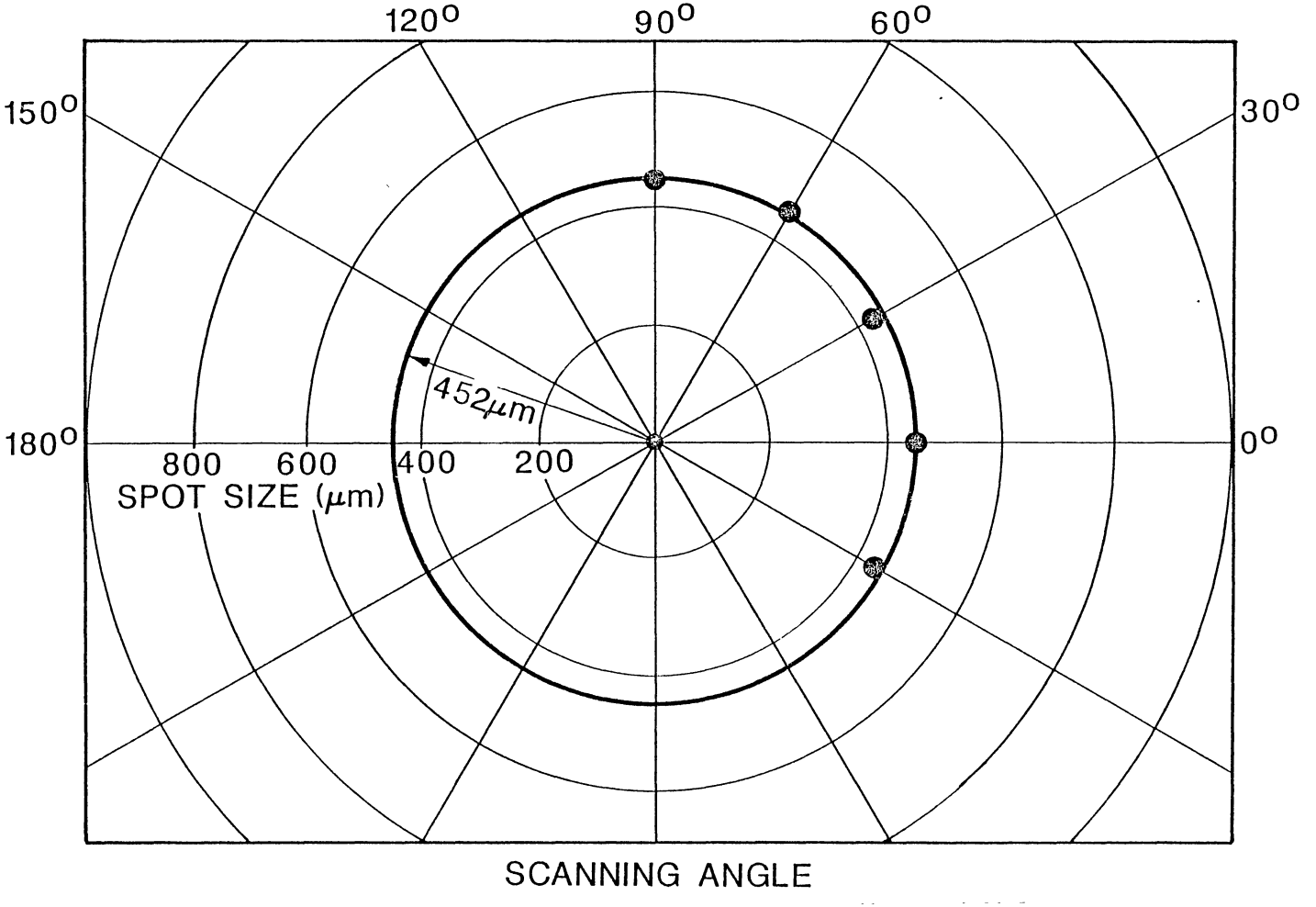

Figure 8. Ellipticity of source beam; note how closely the measured points fit on a drawn circle of 452 um radius.

Waist size and location

The laser waist size and location can be determined by measuring the spot sizes at various distances from the laser and fitting spot size vs distance into the relationship:

$$w(z) = w_o \sqrt{1 + \frac{(z-z_w)^2}{(\pi w_o^2 / \lambda)}} \qquad (2)$$

where w_o the waist size (the minimum spot size, and where the phase-front is almost planar) and z_w the waist location, are the parameters to be determined. w(z) is the spot size at location z.

Measurements were made along the x-axis only, as the beam was considered to be roughly circular in shape. Spot sizes were measured at five different locations, and the resulting least-squares fit gave the size of the waist as 330 $\pm$ 2 um and the location as 26 $\pm$ 5 mm behind the front end of the housing and inside the laser cavity.

Frequency characteristics

The output frequency spectrum of the laser was analyzed using a Coherent 240-2-B laser frequency analyzer. The analyzer consists of two mirrors contained at the ends of a cavity in a confocal arrangement. One of the mirrors is connected to a piezo-electric transducer to which a sawtooth waveform voltage from an oscilloscope time-base is applied. Application of this voltage causes the mirror to move and the length of the cavity consequently changes. Since, to

resonate, the cavity length has to be an integer number of wavelengths of the input frequency of the light, this causes the resonance frequency of the cavity to change.

If light enters the scanner at a resonance frequency, maximum transmission through the cavity will occur, and the output can be measured by a detector placed at the other end of the frequency analyzer. The detector can be connected to an oscilloscope to visually show the frequency spectrum. A frequency scan through a range of frequencies can be made continuously by application of the sawtooth voltage.

From the specifications, the resolution of the scanner (ratio of optical frequency to instrument bandwidth) is given as $8x10^6$, and the free spectral range is 1500 MHz; the finesse (see appendix A) is given as 200.

A frequency scan of the laser beam (Figure 9) shows it indeed to be a single frequency TEM00 mode. This can be inferred from the fact that there is a single peak within the free-spectral range, and that the output of the laser is a single dot. The finesse, (free spectral range) / (full-width at half maximum), of the laser is determined from the curve to be 120 (see Appendix A), which is most probably imposed by the scanner .

The laser is suitable for use as a source for injection. Any excitation of Hermite-Gaussians in the ring resonator would have to be caused by a single-frequency fundamental Gaussian, since the source apparently has no visible Hermite-Gaussians in its spectrum.

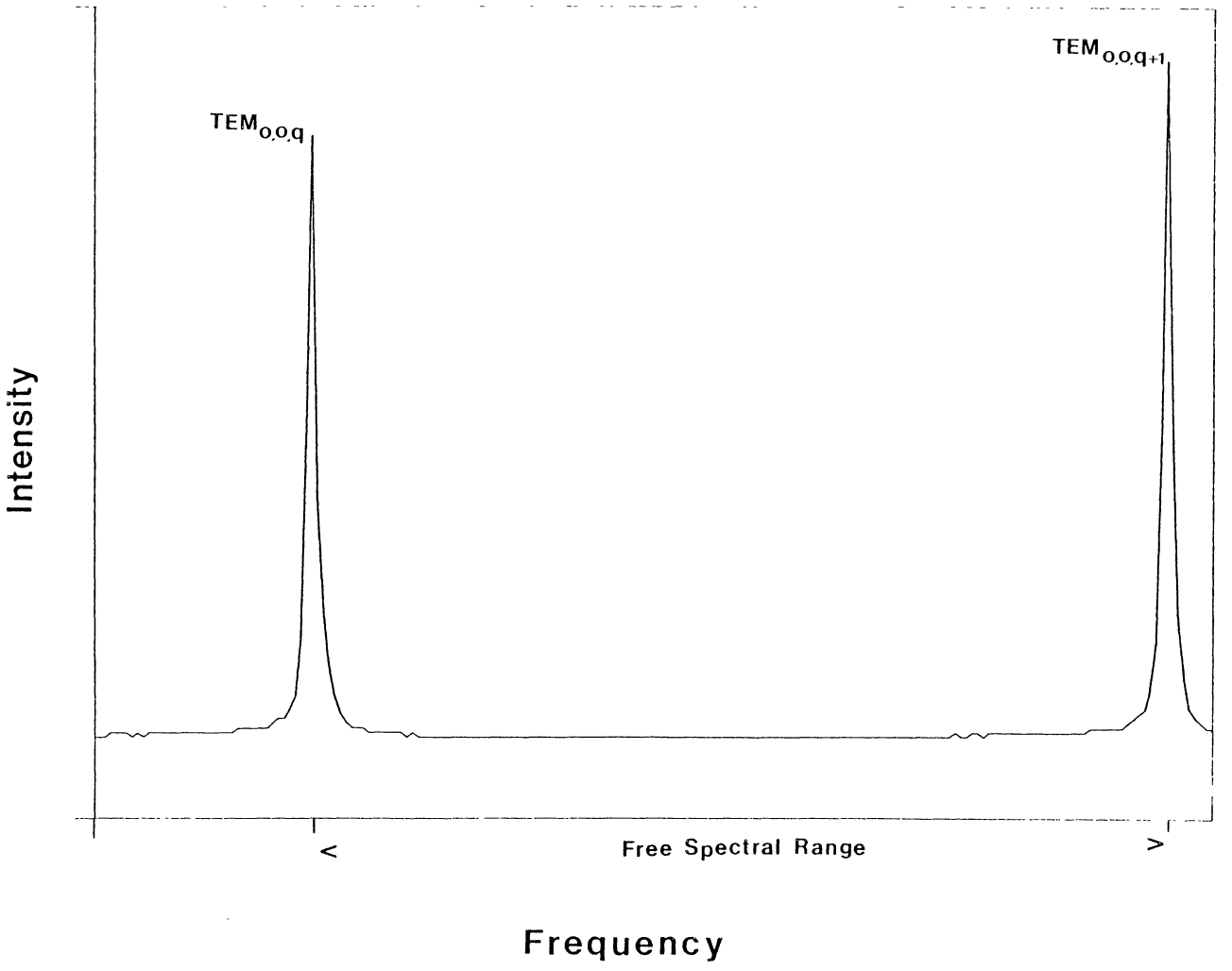

Figure 9. Measured frequency scan of source beam using an optical spectrum analyzer; results indicate the presence of a single mode only.

CHAPTER III

SETUP OF THE RING RESONATOR

Construction of the Ring

The ring resonator was constructed from four mirrors of 5 m radius of curvature mounted on mirror holders having and angle adjustments as shown in Figure 1Ø. The assembly was done on a 3 ton granite block measuring 9 feet by 6 feet by 8 in. and having a smooth top, with an RMS height variation of less than 1 mm.

First a square of the required length was marked out on the block, then mirrors mounted on the mirror holders were placed with centers approximately on the corners of the square so that the normals to the mirror surfaces would subtend an angle of 45^{o} to a side. Adhesive was then applied to fix the holders to the table surface. One side of the square was drawn out and extended to provide a reference for source injection. This arrangement proved to be satisfactory to get the ring aligned.

Output from the ring was taken from the mirror diagonally opposite the injection mirror; The height of the ring was about 6.3 cm above the table surface, and an arrangement of mirrors had to be used to feed the resonator output to the frequency scanner.

Basically, two rings were constructed, one which was 1 m on a side and another 15.4 cm on a side, using the same mirrors. The larger ring appeared to be more unstable so most observations were made on the smaller ring.

The mirror radii as measured in the lab were: $R_a = 5.Ø1 \pm .Ø1$ m, $R_b = 4.95 \pm .Ø3$ m, $R_c = 5.12 \pm .Ø2$ m, $R_d = 4.95 \pm .Ø3$ m ; all values were reasonably close to 5 m , so for ease of calculation, all four mirror radii were assumed to be 5 m.

Various analyses were performed before construction, among which were the focusing stability, the eigenmodes and waist size and location, and the finesse of the cavity.

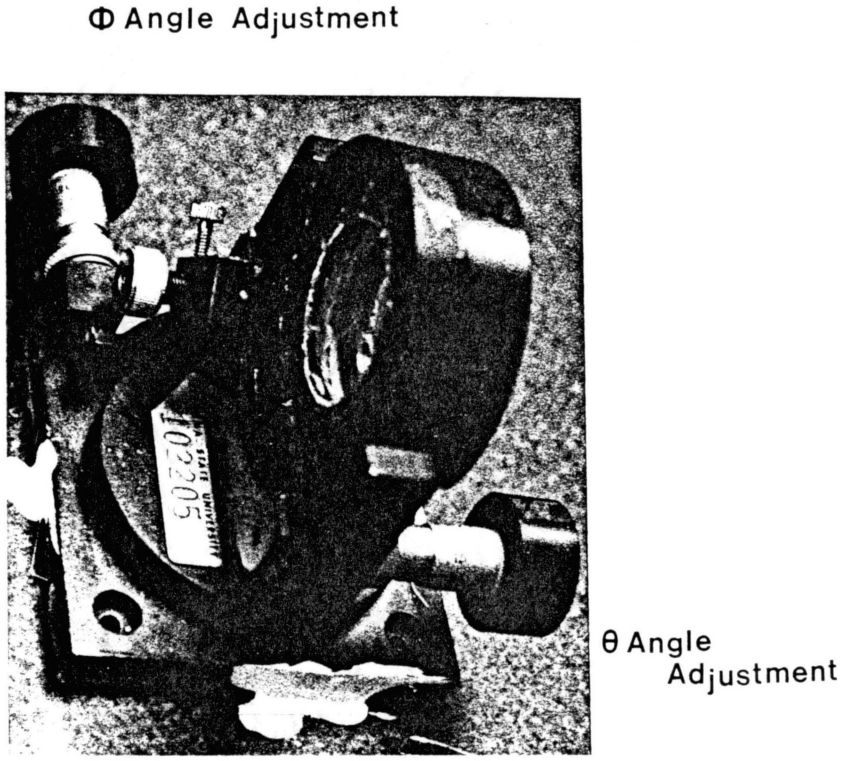

Figure 1Ø. Mirror holder used at one of the four corners of the ring; knobs providing angular adjustments are indicated.

Mirror reflectivity

In order to be able to predict the finesse of the ring, mirror reflectivities had to be measured for all four mirrors. This was done in a separate experiment by feeding a beam from a laser onto a mirror surface and measuring the amount of power P_t that passes through the mirror. Since the laser power output P_o is known and is constant over time, the transmittivity T of the mirrors is given by $T = P_t/P_o$.

Since the mirrors are of a multilayer dielectric configuration, it is assumed that the power absorbed is very small. It is also assumed that light scattered from the mirrors is negligible. Reflectivity R is then given by $R = 1 - T$.

The mirrors were designed for maximum reflectance at $\emptyset^o$ incidence (the angle which the normal of the mirror subtends with the input beam), so the reflectivity had to be measured in a range of incidence angles around 45^o, which is the angle at which the beams would actually hit the mirrors inside the resonator. Reflectance at $\emptyset^o$ was found to be ~ 99.9% .

Unfortunately, it was found that the reflectivity decreased as the incident angle increased; at 45^o incidence the reflectivity was between 99.8 and 99.7 % for all four mirrors. Mirror reflectivities for all calculations were then taken from the curves in Figures 11 and 12.

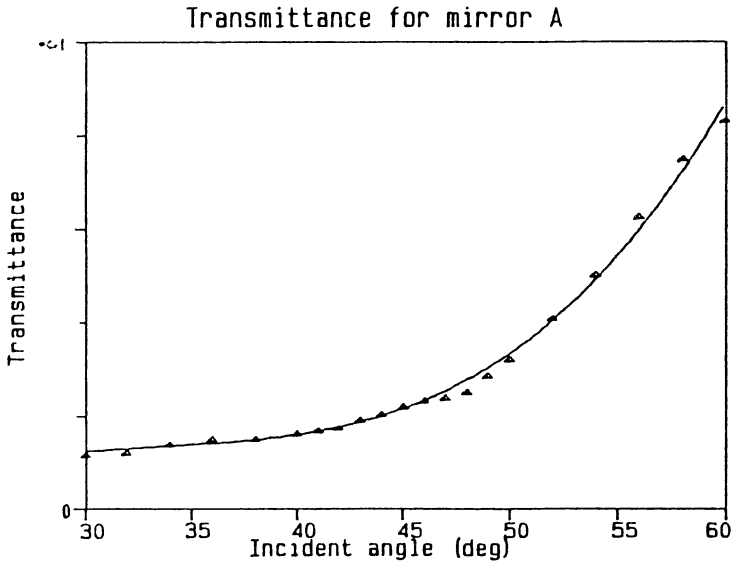

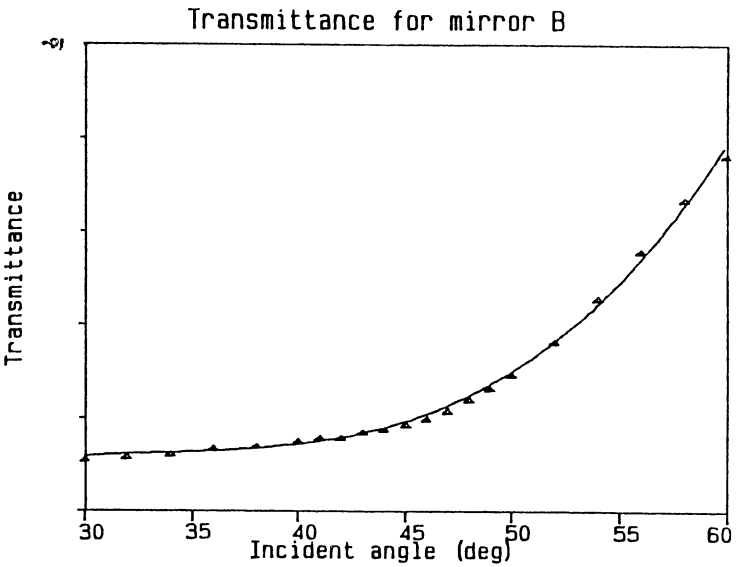

Figure 11. Transmittance vs incident angle for mirrors A and B.

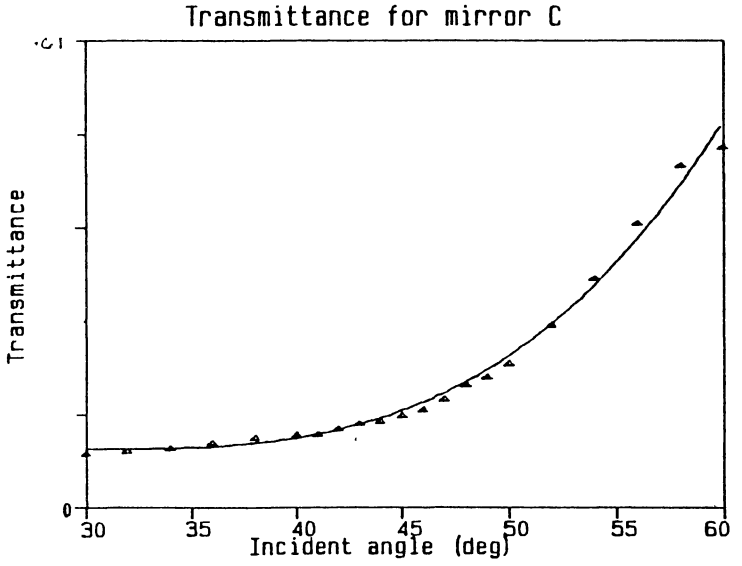

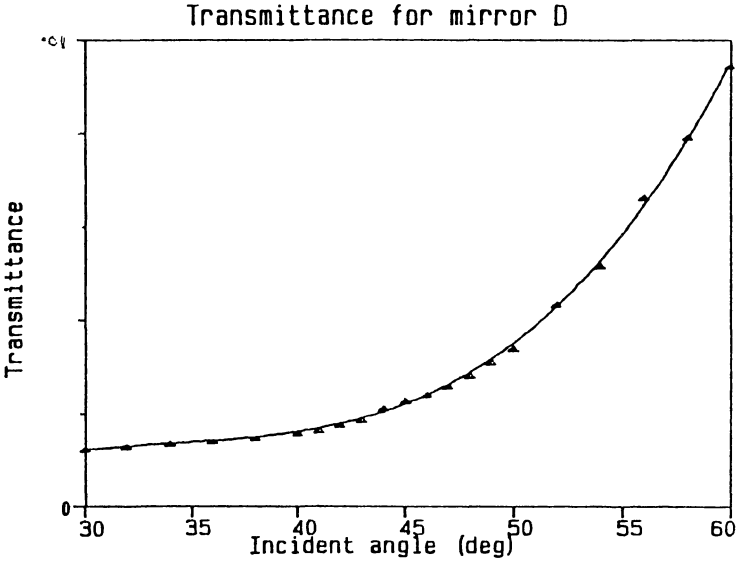

Figure 12. Transmittance vs incident angle for mirrors C and D.

Geometry of the Optical Axis

The actual length of the resonator, which is the length of the round trip optical axis, had to be determined after injecting a source beam and getting the ring to resonate. Once resonance was achieved, the length of a side could be measured by laying a scale inside the ring and parallel to a side and moving a vertical straight edge on the scale till it intersected a beam. Assuming the ring is an approximate square, the difference on the scale between the two points when a beam is encountered gives the length of a side.

Obviously, the ring will not resonate once a beam in one of its legs is blocked, but it is assumed that in a well aligned system, the non-resonating and the resonating beam-path are the same. Measurements with an error of about a quarter millimeter could be made by using this method.

To calculate angles, the diagonals were measured directly by placing a scale on top of the mirror holders and reading off the distances between marks on top of the holders indicating the surface of the mirrors. It was assumed that there was an error of measurement in diagonal AC by e_1 and in diagonal BD by e_2 (see Figure 13). A set of the smallest values for these errors were then calculated to make the sum of the angles at the corners equal 360°. The values chosen for the errors were $e_1 = e_2 = 0.028$ cm, well within the errors expected in the measurement of the diagonals.

The tilt of the optical axis to the table surface was determined by measuring the beam height at various points. The difference in height between the highest and lowest points was found to be less than 1 mm . Strictly speaking, it cannot be assumed that the optical axes lie in a single plane.

The following data were determined for the ring:

Length of side AB = 15.5Ø cm

Length of side BC = 15.7Ø cm

Length of side CD = 15.35 cm

Length of side DA = 15.2Ø cm

Length of diagonal AC = (22.1 + Ø.Ø28) = 22.13 cm

Length of diagonal BD = (21.5 + Ø.Ø28) = 21.53 cm

Angle at A = 88.1°

Angle at B = $9Ø.3^{\circ}$

Angle at C = 87.8°

Angle at D = 92.8°

Sum of angles = $36Ø.Ø^{\circ}$

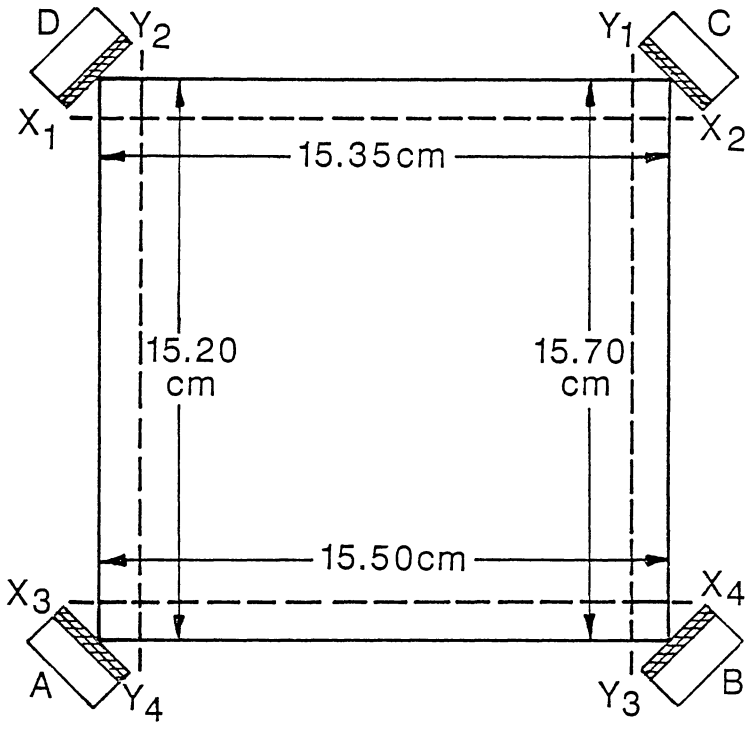

Figure 13. Measured lengths of sides of the ring; the points Xi and Yi indicate when the straight edge encountered a beam.

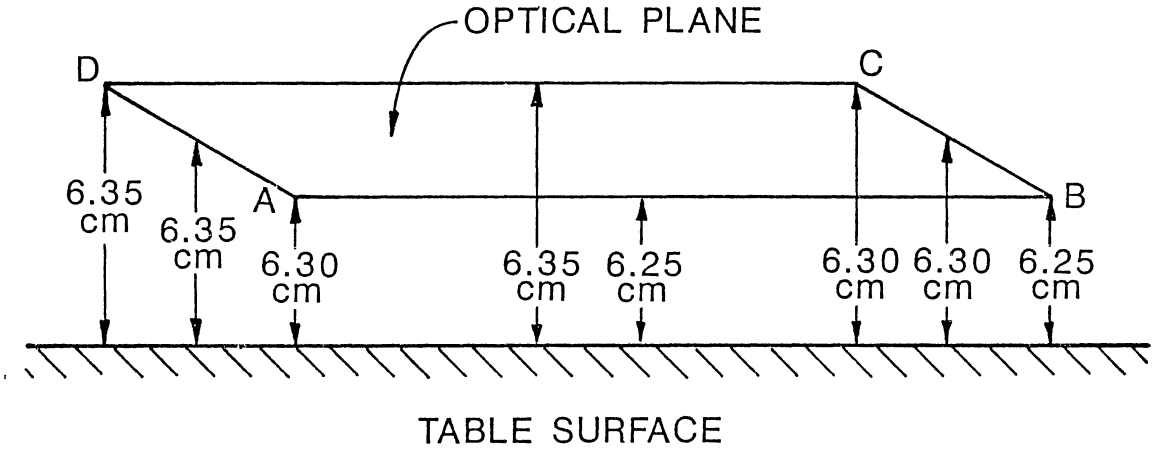

Figure 14. Tilt of the optical axis with reference to the table surface; errors were less than 1/4 mm.

Calculation of finesse

A transmission analysis for the quadrilateral resonator is presented based on a similar analysis in (Haus, 1984) for a linear Fabry-Perot etalon (interferometer).

In the analysis, θ is the incident angle, S is the distance between mirrors, ω is the frequency of the wave, r_a represents the reflectivity of mirror A; t_a is the transmittivity of mirror A; d_{AB} represents the phase delay of the wave passing through the length AB.

A beam injected with amplitude a_i is transmitted through mirror A with amplitude $jt_a a_i$. The wave then arrives at mirror B phase-shifted by an amount $\omega n(\cos\theta S)/c = d_{AB}$. The portion of the wave reflected from mirror B is given by $-r_B(jt_A)(e^{-jd}a\ a_i)$. This reflected portion arrives at mirror C phase-shifted by an amount $\omega n(\cos\theta S)/c = d_{BC}$, and a part of this is transmitted through C. The expression for the amplitude of the wave transmitted through C for the first pass through the loop is given by :

$$-r_B(jt_A)(jt_C)\ e^{-j(da+db)} = r_B(t_A)(t_C)\ e^{-j(da+db)}$$

The reflected wave from C goes round the loop and returns at C, and the same process is repeated over. The final expression for the total amplitude output a_f from C is given by an infinite geometric series :

$$a_f = r_B t_A t_C e^{-jd} + j(t_A)[(-r_B)(-r_C)(-r_D)(-r_A)](-r_B)(jt_C)e^{-j(d+P)} + \ldots$$

$$a_f = r_B t_A t_C e^{-jd} \cdot$$
$$[1 + \{(r_B)(r_C)(r_D)(r_A)\} + \{(r_B)(r_C)(r_D)(r_A)\}^2 + \ldots]\, a_i$$

P = perimeter of the ring.

Using the relation for an infinite geometric series :

$$a_f = \frac{t_A r_B t_C e^{-j(dA+dB)}}{1 - r_B r_C r_D r_A e^{-jd}} \qquad (3)$$

where d represents the phase delay around the entire perimeter of the ring (one round trip).

The total power transmitted (in watts) is given by:

$$I_o = |a_f|^2 = a_f a_f^*$$

$$I_o = \frac{t_A^2 r_B^2 t_C^2 |a_i|^2}{(1 - r_B r_C r_D r_A)^2 + 4 r_B r_C r_D r_A \sin^2(d/2)} \qquad (4)$$

For this particular ring,

$r_A = .998, \quad r_B = .998, \quad r_C = .998, \quad r_D = .9975$

$t_A = 1 - r_A = 0.002, \quad t_C = 1 - r_C = 0.002$

$$I_o = \frac{1.594 \times 10^{-7}}{7.179 \times 10^{-5} + 3.976 \sin^2(d/2)}\, I_{in}$$

where $I_{in} = |a_i|^2$

At resonance, the $\sin^2$ term equals zero and the maximum output power is given by:

$$I_o = \frac{1.594 \times 10^{-7}}{7.179 \times 10^{-5} + 3.976}\, I_{in} = 2.22 \times 10^{-7}\, I_{in}$$

The finesse can be calculated from (Appendix A):

$F = 4R^{1/2}/(1-R) = 47Ø$

where $R = r_A r_B r_C r_D$

The Free Spectral Range (FSR) is given by c/P where P is the perimeter of the ring.

$FSR = 3x1Ø^8 / .6175 = 486$ MHz

Since the FSR of the available spectrum analyzer is given as 15ØØ MHz, it should be possible to measure the finesse quantitatively, if resonance can be established.

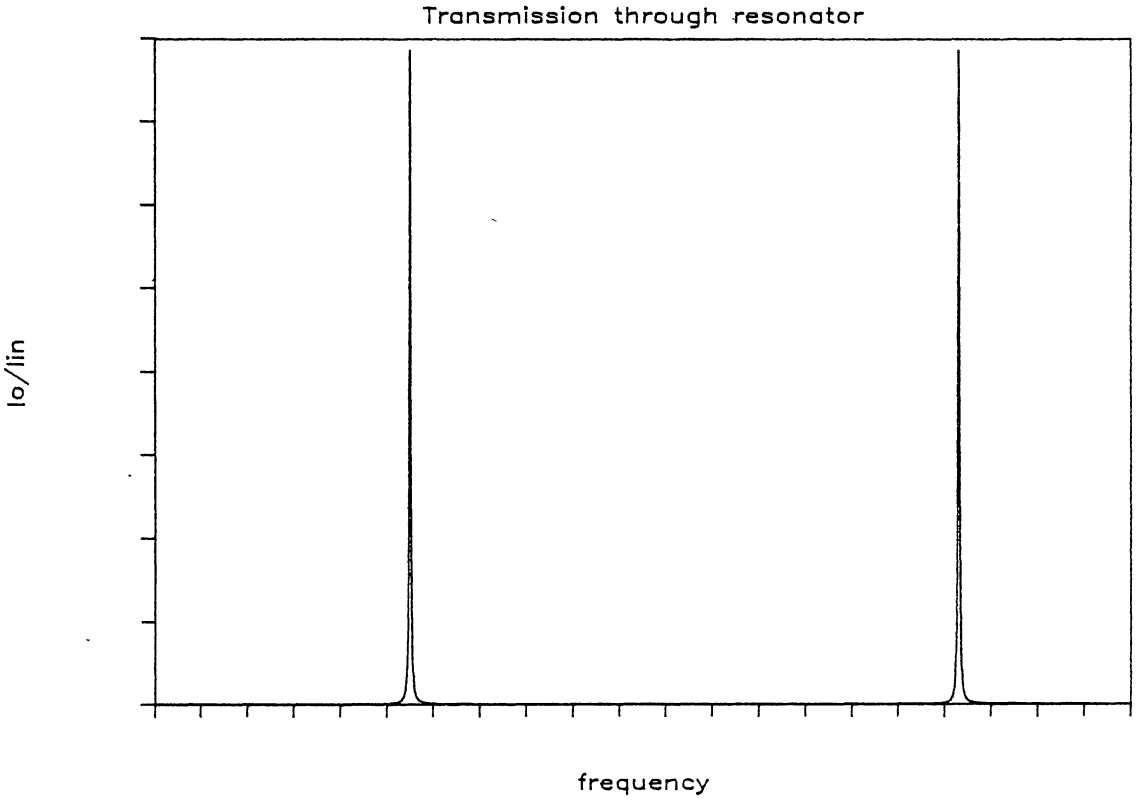

Figure 15. Result expected from a frequency scan of the resonator; the scan was generated using calculated power ratios.

Eigenmodes of the ring

To obtain the fields everywhere inside an open optical resonator, we use Huygens Principle with certain approximations to give the following integral (Siegman, 1971) We use an xyz coordinate system with wave propagation along the z-axis.

$$\tilde{u}(x,y,z) = \frac{je^{-jkz}}{z\lambda} \int_s \int \tilde{u}_o(x_o,y_o) e^{-j(k/2z)[(x-x_o)^2+(y-y_o)^2]} \cdot dx_o dy_o \quad (5)$$

$\tilde{u}(x,y,z)$ = complex wave amplitude anywhere inside resonator

$\tilde{u}(x_o,y_o)$ = complex wave amplitude at input plane

s = coordinate on surface of input plane

x_o , y_o = input plane

where z replaces L , the length of the resonator , assuming $z_o = \emptyset$ at the input plane.

In resonators which exhibit higher-order modes, Hermite-Gaussians are most commonly found to be present. One of many different solutions, the Hermite-Gaussian solution to this integral is given by: (Haus, 1984)

$$U_{mn}(x,y,z) = \frac{C_{mn}}{\sqrt{\left[1 - z^2/z_o^2\right]}} \psi_m\left[\frac{\sqrt{2}x}{w_x}\right] \psi_n\left[\frac{\sqrt{2}y}{w_y}\right] \cdot \quad (6)$$

$$\exp\left[\frac{-jk}{2R}(x^2+y^2)\right] \exp\left[j(m+n+1)\phi\right]$$

where

$$C_{mn} = \left[\frac{2}{w_o^2 \, \pi \, 2^{m+n} \, m!n!} \right]^{1/2}$$

$$\psi_\eta(\xi) = H_\eta(\xi) e^{-\xi^2/2}$$

all other parameters are as defined before.

Assuming the Hermite-Gaussian solution above, we can define a q parameter which can completely represent a mode of any order . The q of a Gaussian beam is a complex parameter which describes the variation in intensity on a plane normal to the optical axis, as well as the curvature of the wavefront, and is given by :

$$q = z + jz_o \; ; \quad 1/q = 1/(z + jz_o) = 1/R - j\lambda/\pi w^2 \qquad (7)$$

where R is the radius of curvature of the wavefront, and w is the spot size. Lambda is the wavelength.

The q parameter can be used to describe transformations of Hermite-Gaussian modes through free-space, lenses and mirrors. The result of these optical components are completely described in (Haus, 1984, page 129). Each of the above mentioned optical components can be represented by ABCD matrices (Haus, 1984, page 131). The matrices described below are used in the ring analysis which follows.

$$\begin{bmatrix} 1 & S \\ \emptyset & 1 \end{bmatrix}$$

Free space of distance S

$$\begin{bmatrix} 1 & \emptyset \\ -2/R_o & 1 \end{bmatrix}$$

Mirror of radius R_o

A good check on q-transformations by matrices is that

$$\det. \begin{bmatrix} A & B \\ D & C \end{bmatrix} = 1 \qquad \text{where} \quad \begin{bmatrix} A & B \\ C & D \end{bmatrix}$$

represents the cascade matrix for a series of elements.

The q parameter is transformed into q' where

$$q' = \frac{Aq + B}{Cq + D}$$

Propagation of the q

A complete analysis of the ring is presented; ABCD matrices are used throughout. To clear up nomenclature, the radius of curvature of a beam or mirror is called positive if it is concave in the direction of the beam.

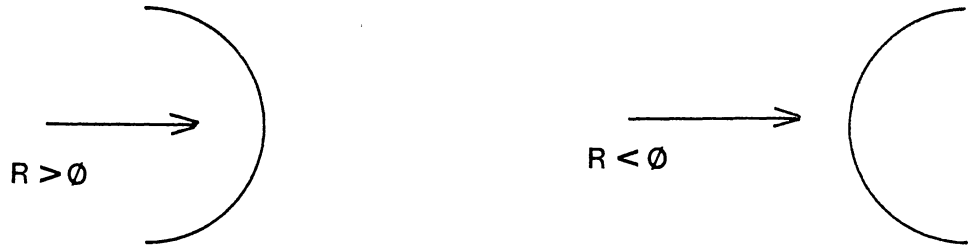

Since beams are obliquely incident on mirrors, the resonator is astigmatic (i.e. the q will propagate

differently in the x-plane (that of the ring) and the y-plane (normal to that of the ring). Call these q's q_x and q_y . For a q to resonate in the cavity, it must repeat after one round trip.

The effective focal length of a mirror for a sheath of rays in the x-plane is $(R/2)\cos\theta$, and in the y-plane is $(R/2)/\cos\theta$ where R is the radius of curvature of the mirror (Bilger, 1985b)

$$f_{Ax} = (R_A/2)\{\cos(\theta_A/2)\} \qquad f_{Ay} = (R_A/2)/\{\cos(\theta_A/2)\} \qquad (8)$$

where the subscript A stands for mirror A.

We form a matrix for one leg of the resonator consisting of a length S, and then a mirror. This matrix is given by :

$$\begin{bmatrix} 1 & S \\ 0 & 1 \end{bmatrix} \begin{bmatrix} 1 & 0 \\ -1/f & 1 \end{bmatrix} = \begin{bmatrix} 1 & S \\ -1/f & 1-S/f \end{bmatrix}$$

Length Mirror Leg

The ABCD matrix for the ring is then obtained by multiplying these four matrices starting from mirror A and travelling anticlockwise. All four mirror radii were taken to be 5 m as mentioned before.

Assuming θ_A = 1/2(angle at A); for the plane of the ring (x-plane):

$$\begin{bmatrix} A & B \\ C & D \end{bmatrix}_{A_+} =$$

$$\begin{bmatrix} 1 & .155 \\ -.561 & .913 \end{bmatrix} \begin{bmatrix} 1 & .157 \\ -.567 & .911 \end{bmatrix} \begin{bmatrix} 1 & .154 \\ -.555 & .915 \end{bmatrix} \begin{bmatrix} 1 & .152 \\ -.580 & .912 \end{bmatrix}$$

$$= \begin{bmatrix} .5195 & .4809 \\ -1.794 & .2300 \end{bmatrix}$$

As a check, the determinant should be 1

The q is then given by :

$$q = \frac{Aq + B}{Cq + D} \qquad \text{or} \qquad q = \frac{AD}{2C} + \sqrt{\frac{(A+D)^2}{4C^2} - \frac{1}{C^2}} \tag{9}$$

substituting the values of A B C D from the cascade matrix, we get:

$$q_x(A_+) = -0.0807 + j0.5167$$

For a plane normal to that of the ring:

$$\begin{bmatrix} A & B \\ C & D \end{bmatrix}_{A_+} = \begin{bmatrix} .5195 & .4809 \\ -1.794 & .2300 \end{bmatrix}$$

$$q_y(A_+) = -0.0773 + j0.7344$$

Since the ring has 4 equally curved mirrors and is approximately symmetric, there will be 4 x-waists and 4 y-waists. A waist can be obtained by adding a straight section to the q at any mirror so the the real part disappears.

$q_x(A_+)$ + Ø.ØØ8Ø7 = jØ.5167 ; w_{ox} = 323 um

$q_y(A_+)$ + Ø.Ø773 = jØ.7344 ; w_{oy} = 385 um

where w_{ox} and w_{oy} are the waist sizes in the x and y planes. Details of the ring along with the waists are shown in Figure 16 on the next page.

The stability of the ring is given by $1-(A+D)^2/4$ and should be between Ø and 1 for a unique q.

(Focusing) Stability_x = Ø.88

(Focusing) Stability_y = Ø.56

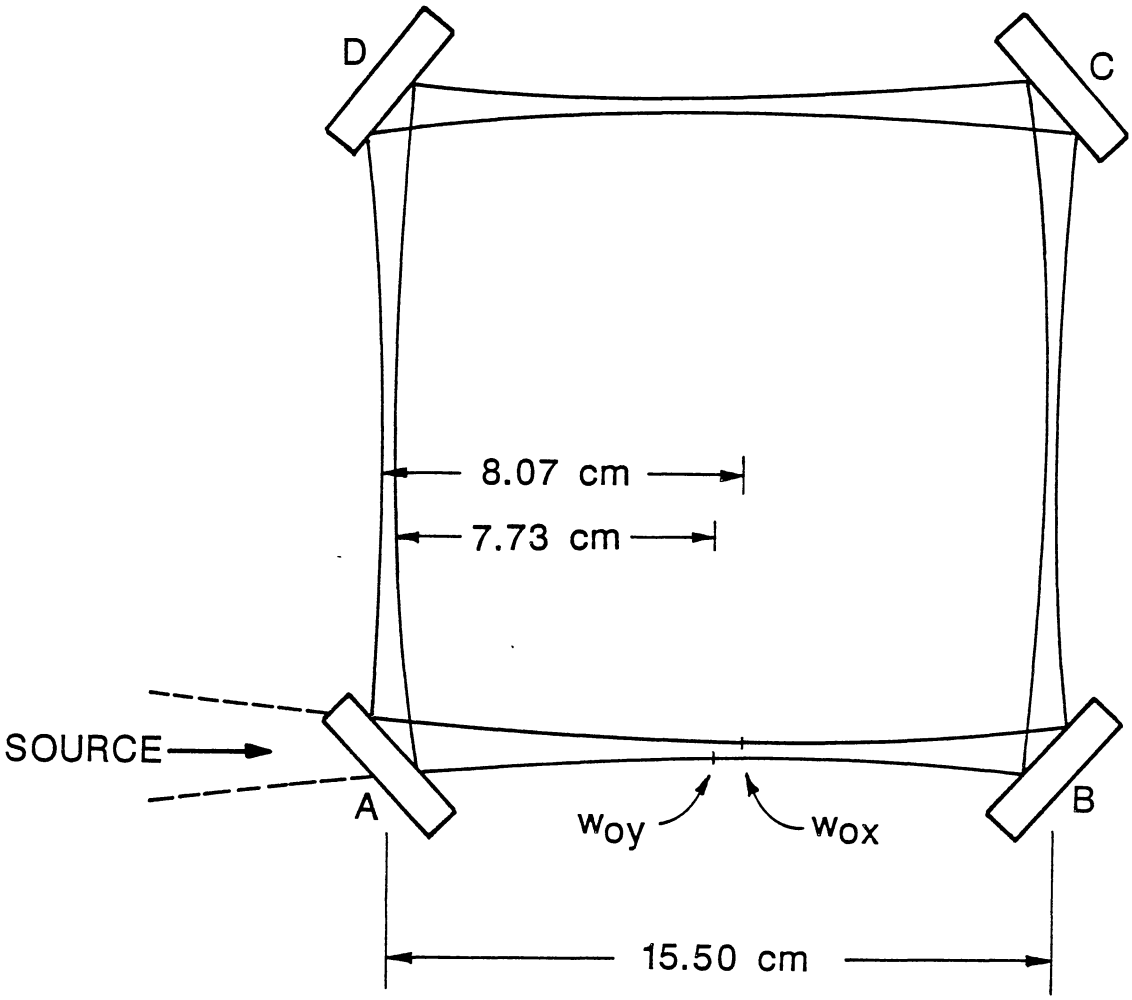

Figure 16. Location of waists in the resonator; there are 4 x-waists and 4 y-waists in each of the legs, but only the two waists in leg AB are indicated. w_{ox} = 323um; w_{oy} = 385um.

Mode matching with input laser

To assure proper resonance , the spot-size and the radius of curvature of the source beam (q_L) have to be matched with the same of the resonators eigenmode. This can usually be accomplished by a lens placed between the laser and the input mirror, and is known as 'mode-matching', although it should more appropriately be termed 'q-matching'

Due to astigmatism, the q_x and q_y of the resonator's eigenmode are different while the source beam is usually non-astigmatic, so cylindrical lenses should in principle be used for precise mode-matching (Bilger, 1985b). However, it was calculated that w_{ox} and w_{oy} were close in value, and it has been determined that an error of 1Ø% in mode-matching would result in a loss of power of only 1% into the resonators fundamental mode (Bilger, 1985b, page 1Ø7). Thus the same size (35Ø um) was assumed for both waists and an easily available spherical lens was used to mode-match in both the x and the y coordinates of the ring with less than 11 % error in matching.

The setup is indicated in Figure 17. The distance L between the laser waist and the matching lens is given by the solution to the quadratic equation; (Bilger, 1985b)

$$(w_{oL}^2-w_{oR}^2)L^2 - 2xw_{oL}^2L + [x^2w_{oL}^2+(\pi/\lambda)(w_{oL}w_{oR})^2(w_{oR}^2-w_{oL}^2)] \quad (1Ø)$$

where w_{OL} the laser waist size is 330 um (see Chapter 2).

w_{OR} the ring waist size is taken to be 350 um .

x is the distance between the two waists

The waist site is taken to be 0.077 m inside the resonator from mirror A. The solution for the equation for x = 0.5 m gives us L = 0.281 m (see Figure 17)

The focal length f of the lens is given by :

$$f = \frac{(x-L)w_{oL}^2 - Lw_{oR}^2}{w_{oL}^2 - w_{oR}^2} \qquad (11)$$

f = 0.78 m for the above values.

A computer program for mode-matching was used to select practical L-f combinations; the above was found to be most suitable.

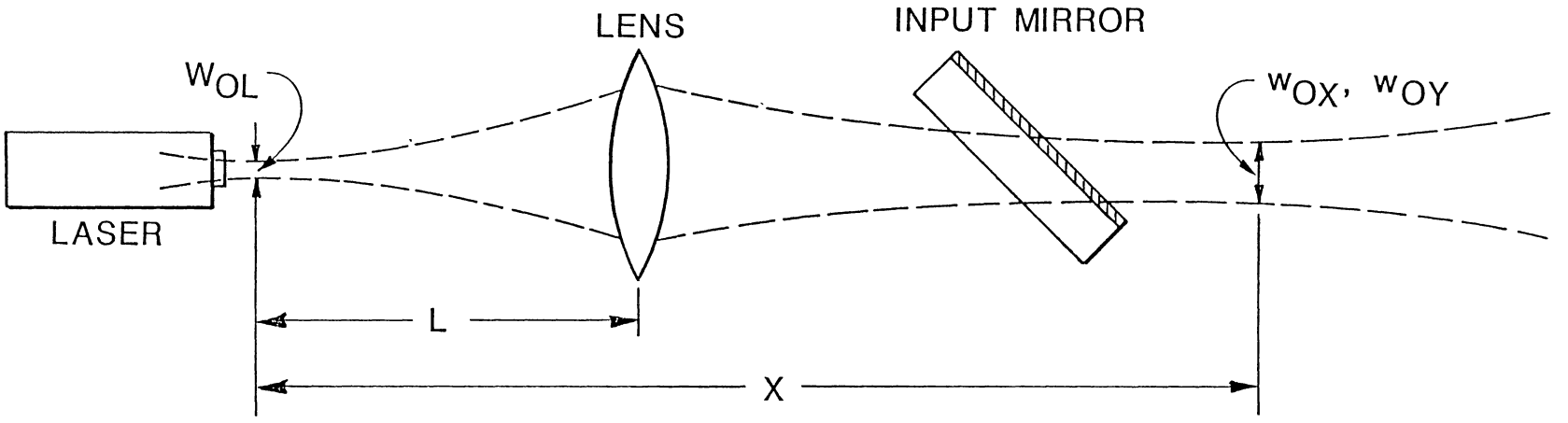

Figure 17. Mode matching of the source with the resonator's q; for this particular construction, L = 28.1cm, X = 50cm.

CHAPTER IV

INJECTION OF SOURCE LASER INTO RING

Injection Through the Beam Aligner

The laser used for injection was mounted inside two optics-holders fixed onto the table surface. A precision beam aligner was then attached at the front end of the laser; this aligner allows for translations and angular tilts of the beam in the horizontal and vertical planes (see Figure 18). The instrument has four adjustment knobs, one for each of the above types of operations, and had to be calibrated for the amount of translation per knob rotation; the angular adjustments were found to be too coarse to use for any kind of fine adjustment.

Calibration of translation was done by use of a straight edge mounted on a vernier and a detector. The edge was fixed to allow about half the beam power to spill over, then one of the translation knobs were rotated a few times to offset the beam. The difference between the old edge position and the new position to again let the same amount of power spill over gave directly the amount of beam translation; this was done in both the x and y directions.

The setup is shown in Figure 18; the results are:

Beam translation per 1 rotation of horizontal adjustment knob $Ø.59 \pm .Ø1$ mm

Beam translation per 1 rotation of vertical adjustment knob $Ø.58 \pm .Ø1$ mm

A vernier on the adjustment knob would allow translations as small as 1Ø um.

Use of the aligner is necessary to precisely inject the source beam along the optical axis of the resonator. It can also be used to investigate the resonator output due to deliberate introduction of offsets and tilts.

To cut off any extraneous radiation around the source's Gaussian (see photographs, Figure 6), an adjustable iris was mounted in the beam path in between the aligner and the mode-matching lens. The iris was adjusted so that power loss was less than 1% .

The complete setup is shown in Figure 19.

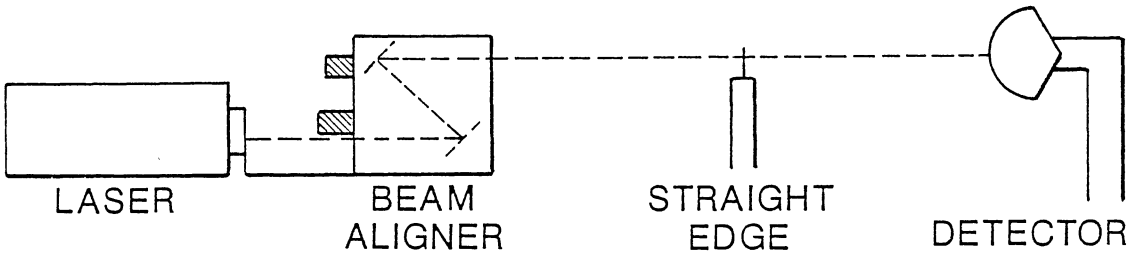

Figure 18. Calibration of the aligner; the straight edge was used to split the beam approximately in half.

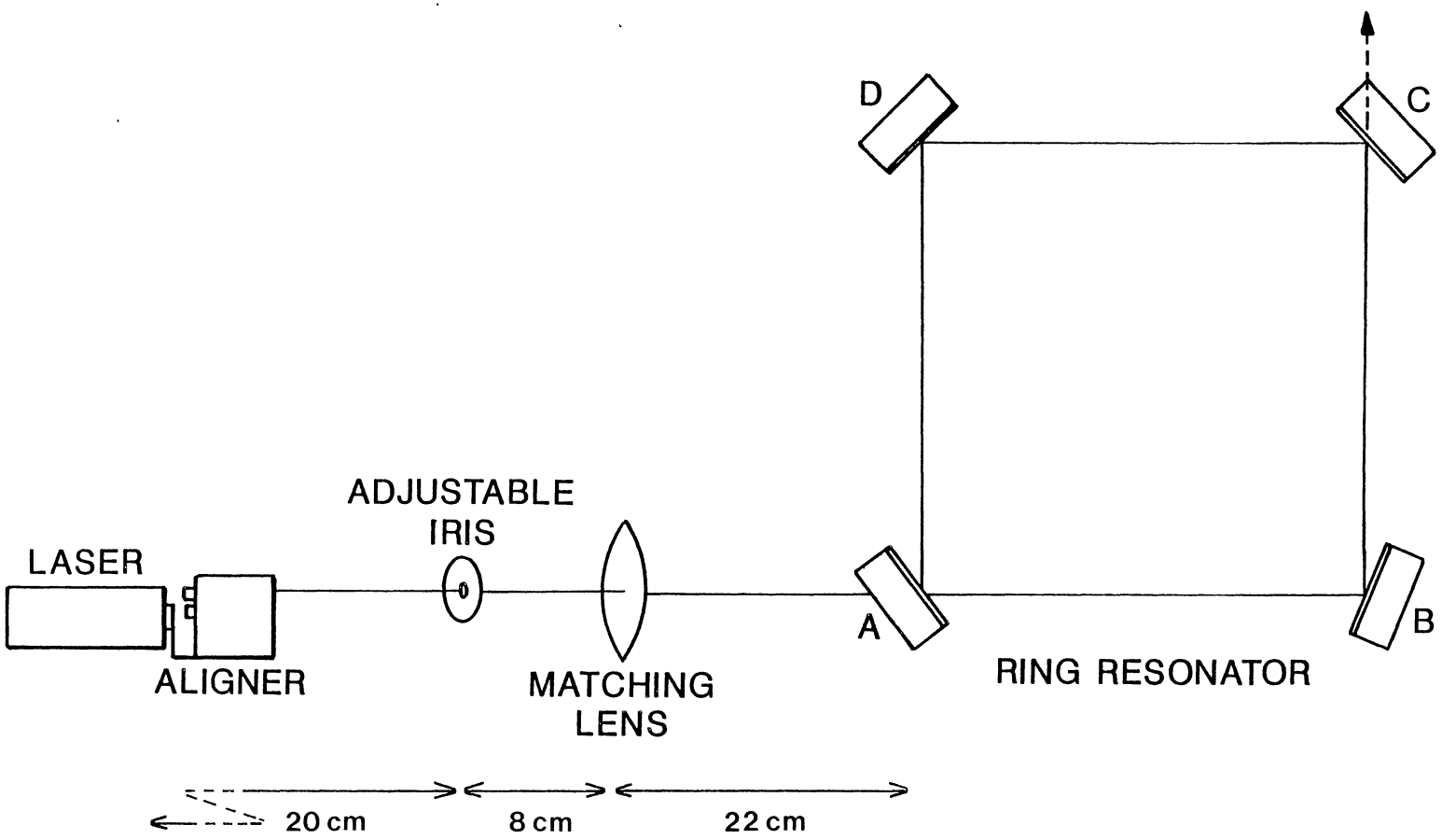

Figure 19. Final setup; note extra distance introduced due to internal reflections off aligner's mirrors.

Adjustment of the Ring

All four adjustments on the beam aligner were used to set the beam path so that it was injected into the optical axis of the resonator. The center of the input mirror was used as reference, and the aligner was adjusted so that after the beam passed through the input mirror (mirror A) it would also hit the approximate center of the next mirror (mirror B). Refer to Figure 19.

Mirrors B, C, and D were then adjusted in turn to keep the beam in the center of the next mirror. Adjustments to the mirrors were strictly in terms of tilts, and were accomplished by using the theta and phi angle adjustment knobs on the mirror holders (see Figure 10).

After the beam would go through one complete round trip and returns to the approximate center of mirror A, two separate spots were visible on mirror B; Mirror A was then adjusted to overlay the two spots on one another. Due to low scattering of the mirrors, the spots are not usually visible, but could be observed by breathing on the mirrors; the condensed vapor which would reveal the beam would evaporate in a few seconds.

After about three rounds of adjustments to overlay the multiple-spots and keep them in the approximate mirror centers, the output intensity of the ring would increase and resonance would begin. Fine-tuning for maximum resonance could be accomplished by delicate adjustments to each of the four mirror holders.

The resonance however, was not found to be very stable; there was an observed fluctuation in power and output pattern. Adjustments to the mirror-holders or to the beam-aligner could not remedy this problem.

Investigation of the Resonator Output

It was not possible to get the output from the ring to stabilize to a single resonance pattern. Two main effects were visible.

1) Variation in power intensity of resonance pattern: It was observed that the ring would sometimes resonate in a single pattern (for example a visually apparent $TEM_{Ø1}$ mode) with increasing intensity till it reached a peak, and then it would decay till perhaps no output at all was visible. This whole event sometimes occurred in the course of a second; the description could possibly be explained by a change in optical path length through the resonance frequency of that particular mode as in a linear Fabry-Perot resonator (Born, 1983).

2) Variation in output pattern:
At times the output pattern would change from, say a Ø,Ø mode to a Ø,1 mode to a 2,2 mode, these modes defined by visually observing the output and comparing it to known Hermite-Gaussian lateral intensity distributions. Photographs taken in the lab of these patterns are displayed in Figure 2Ø.

Over the course of a few seconds, a number of different patterns could be observed, some of which were apparently a mixture of different modes as shown in Figure 2Øc. An explanation proposed for this phenomena is outlined in Chapter 6, and it is suggested that it may be possible for a fundamental Gaussian to excite mainly a higher-order Hermite-Gaussian due to optical path-length changes caused by mirror perturbations. Excitation of higher-order modes by misadjustment of source has also been investigated.

Two sources of error have been proposed:

1) Misadjustment of source with the resonators eigen-mode due to spatial movements of the injection laser.

2) Internal changes of the optical axis due to mirror perturbations caused by thermal changes and vibrations carried through to the setup on the granite block.

A frequency scan of the output could not be satisfactorily accomplished due to output fluctuations; the theoretically calculated finesse of the ring thus could not be verified.

It had been proposed that if the output had been more stable, the frequency content could be studied to reveal the presence of higher-order modes, and changes in their amplitude due to source misadjustment; in other words, an experimental verification of the theoretically proposed scheme (Sayeh, 1985) .

To get an idea of the causes for resonator instability, an extensive literature search was done; it was noted that 'mirror noise' was attributed to be the major factor for instability of optical ring-resonators (Fredricks, 1978), (Yamauchi, 1974), (Al'tshuler, 1977).

Studies were then done on the effects of external (source) and internal (mirror) instabilities and their effects on the resonator output.

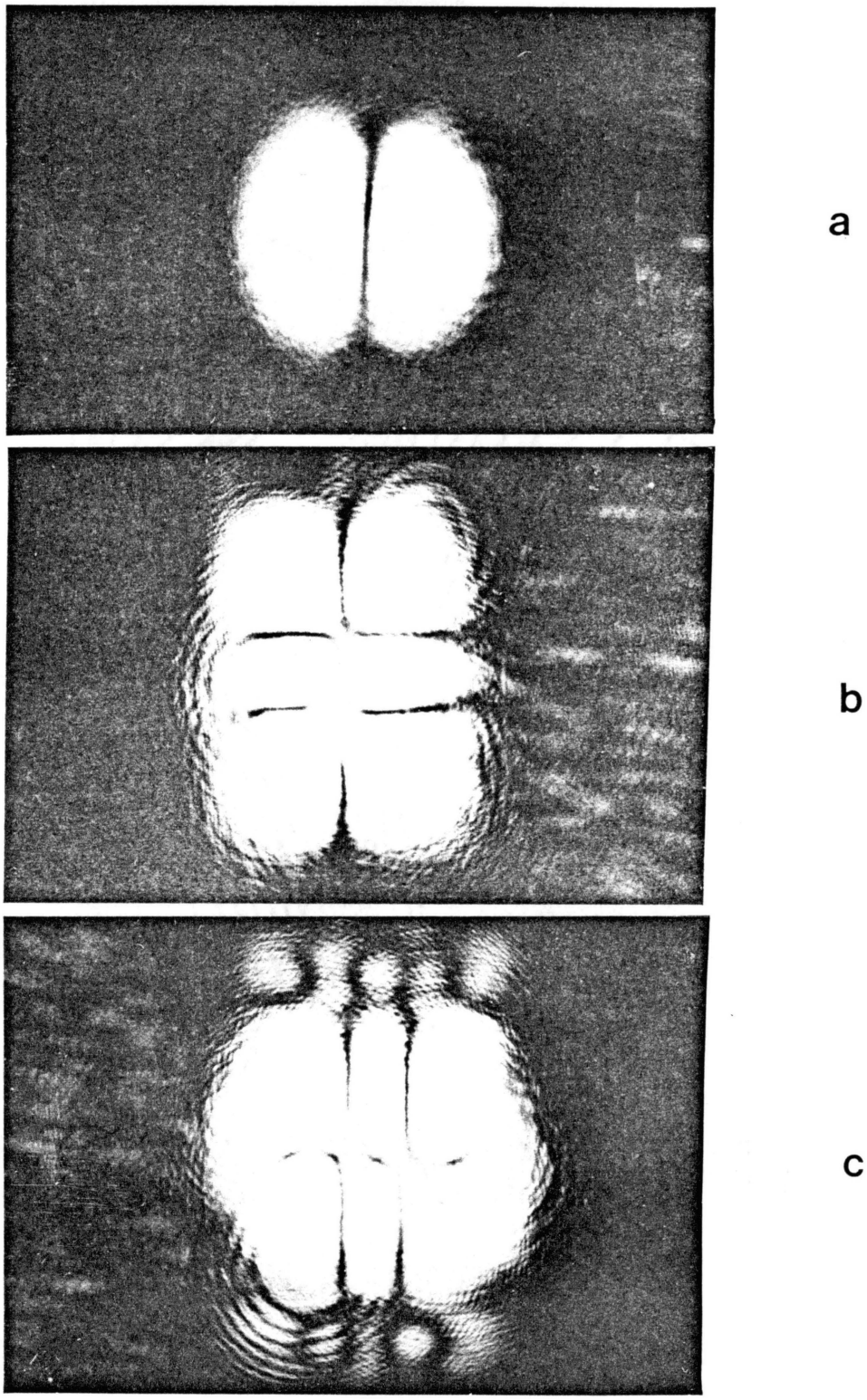

Figure 2Ø. Photographs of resonator output; a) 1,Ø mode b) 1,2 mode c) mixture of a 2,1 mode, and a higher-order mode.

CHAPTER V

EXTERNAL STABILITY

Theory

Fluctuations in the ring resonator output prompted a study into possible causes. Previous investigations (Sayeh, 1985) indicate that it may be possible to excite higher-order modes in a passive resonator by injecting with a misadjusted source beam. Some theory from the above-mentioned paper is presented here.

We refer to the Hermite-Gaussian solution for the Fresnel diffraction integral with approximations (Equation 7).

$$U_{mn}(x,y,z) = \frac{C_{mn}}{\sqrt{\left[1 - z^2/z_o^2\right]}} \psi_m\left[\frac{\sqrt{2}x}{w_x}\right] \psi_n\left[\frac{\sqrt{2}y}{w_y}\right] \cdot$$

$$\exp\left[\frac{-jk}{2R}(x^2+y^2)\right] \exp\left[j(m+n+1)\phi\right]$$

This function can be separated into a product of two functions each of m and n.

$$U_{mn}(x,y) = U_m(x,y)U_n(x,y) \qquad (12)$$

where

$$U_m = \left[\frac{2}{w_x \sqrt{\pi}\, 2^m\, m!} \right]^{1/2} \psi_m\left[\frac{\sqrt{2}x}{w_x} \right] \cdot \exp\left[\frac{-jk}{2q_x} x^2 + j(m+1/2)\phi_x \right] \tag{13a}$$

$$U_n = \left[\frac{2}{w_y \sqrt{\pi}\, 2^n\, n!} \right]^{1/2} \psi_n\left[\frac{\sqrt{2}y}{w_y} \right] \cdot \exp\left[\frac{-jk}{2q_y} y^2 + j(n+1/2)\phi_y \right] \tag{13b}$$

The electric field of a wave of order mn with polarization only along the x-axis is given in (Haus, 1984, page 126) after simplifications and normalization for power

$$E_{mnq}(x,y,z,t) = \sqrt{2\eta P_{mn}}\, U_{mn} e^{-jkz} e^{j\omega t} \hat{x} \tag{14}$$

where P_{mn} is the total power in a longitudinal mode passing through a plane perpendicular to the direction of wave travel.

The functions U_{mn} form an orthogonal and complete set, and therefore so do the functions E_{mnq}. Thus we can expand the x-component of the electric field of the source beam in terms of this set:

$$E_L = \sum_m \sum_n A_{mn} E_{mnq} \tag{15}$$

where the expansion coefficients A_{mn} represent the relative amplitudes of different m,n,q modes.

The expansion coefficients are normalized so that

$$\sum_{m}\sum_{n} |A_{mn}|^2 = \sum_{m} |A_m|^2 = \sum_{n} |A_n|^2 = 1$$

A_μ is given by:

$$A_\mu = \int_{+\infty}^{-\infty} U_\mu(v) U_L(v)\, dv \qquad (16)$$

(where μ = m or n ; v= x or y)

In the analysis it is assumed that a zero-order stigmatic Gaussian beam is used for injection into the resonator.

We define three types of misadjustment:

1) Lateral displacement of the incoming beam with the resonator eigenmodes by ε_x and ε_y in the x and y directions.

2) Angular displacement of the injected beam by α_x and α_y against the resonator z-axis which is also the optical axis.

3) Different waist sizes as well as locations.

ε_x and ε_y are measured in units of spot size; α_x and α_y in units of beam divergence. Figure 22 shows pictorially the types of error.

The following figure shows how misadjustment can be segmented:

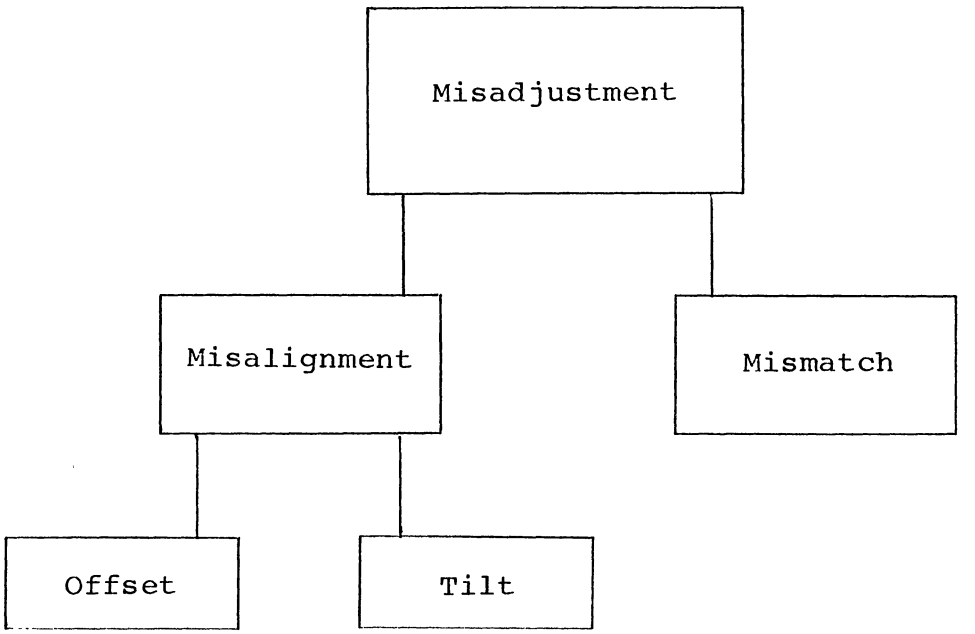

Figure 21. Types of misadjustment.

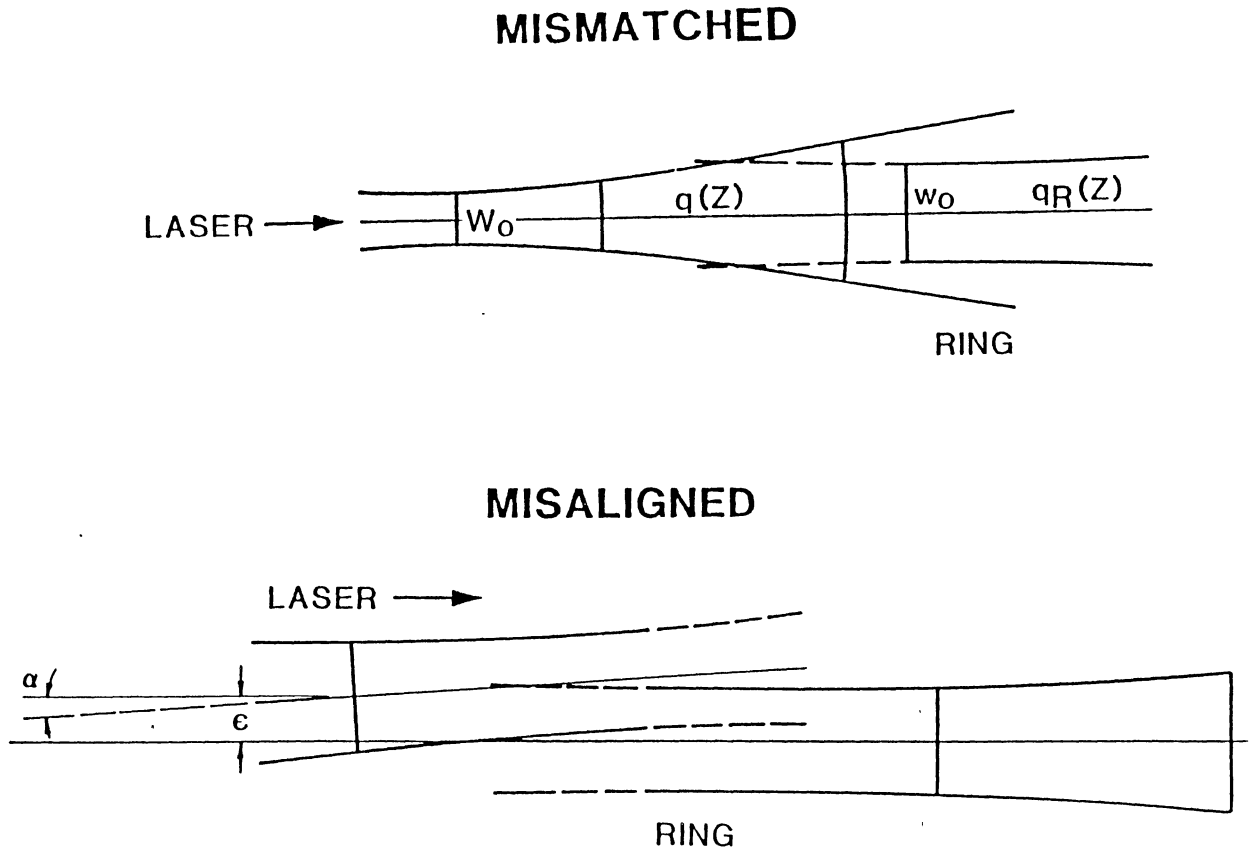

Figure 22. Pictorial representation of mismatch and misalignment along a single axis. W_o represents laser waist size, w_o represents ring waist size.

For ease of analysis we define two parameters; a misalignment parameter which indicates the amount of lateral as well as angular displacement, and a mismatch parameter which gives the waist size and site errors.
These parameters are given by:

Misalignment parameter:

$$\xi_{\upsilon} = \varepsilon_{\upsilon}/w_{r\upsilon} + q_{\upsilon}/w_{r\upsilon}\,\alpha_{\upsilon} \tag{17}$$

Mismatch parameter:

$$\square_{\upsilon} = \sqrt{\frac{q_{\upsilon}^{*} + q_{L}}{q_{\upsilon}^{*} - q_{L}}} \tag{18}$$

where

$w_{r\upsilon}$ = waist size in ring

q_{υ} = q of ring at (ring's) waist

q_{L} = q of laser at (laser's) waist

The coordinate system of the resonator is used as a reference and it is assumed that the coordinate system of the laser is tilted and offset. The resonator's coordinate system, xyz, comprises of:
The x-coordinate, which is in the plane of the ring; the y-coordinate, which is perpendicular to the plane of the ring, and the z-axis which is identical to the optical axis or beam center.

The coordinate system of the laser is given by x'y'z' with similar definitions.

After lengthy calculations using coordinate transformations with certain approximations, we can express the electric field of the laser in terms of the unprimed coordinates as:

$$E_{mnq}(x,y,z,t) \approx \sqrt{2\eta P_L}\, U_L e^{-jkz}\, e^{j\omega t}\, \hat{x} \tag{19}$$

where E_L is given by Equation 15,

P_L is the total power in the laser,

$U_L(x,y)$ is expressed in terms of the misadjustment parameters

Using these definitions, we can express the amplitudes in the form:

$$A_\mu = \int_{+\infty}^{-\infty} U_\mu(v) U_L(v)\, dv = W_v \equiv_v M_{\mu v} \tag{20}$$

where

$$W_v = \left[1 - \sigma_v^2\right]^{1/4}$$

$$\equiv_v = \exp\left[-q_v/q_{Lv} \left(\varepsilon_v^2/w_v^2 - (1+\sigma_v^2)\xi_{v/2}^2 \right) \right]$$

$$M_{\mu v} = \left(2^\mu \mu!\right)^{-1/2} \sigma_v^\mu H_\mu\left[\xi_v(1+\sigma_v^2)/(\sqrt{2}\sigma_v)\right]$$

also

$$A_{mn} = W_x W_y \equiv_x \equiv_y M_{nx} M_{my}$$

where $M_{0v} = 1$

As a check, we see that $A_{\emptyset} = 1$ and $A_{\mu} = \emptyset$ for perfect match and alignment.

Power Transfer into the Resonator's Eigenmodes

To find the power transferred into a certain mode, we can use the ratio of the amplitude for that mode to the amplitude of a zero-order mode. The square of the absolute value of this ratio then gives the relative power transferred into that mode, and can be confirmed by measuring the ratio of the peaks directly from the frequency spectrum.

The amplitude ratios are given by:

$$A_{\mu}/A_{\emptyset} = M_{\mu\nu} = \left(\square_{\nu}^{\mu} 2^{\mu/2} \sqrt{\mu!}\right) H_{\mu}\left[\xi_{\nu}(1+\square_{\nu}^{2})/(\sqrt{2}\square_{\nu})\right] \qquad (21)$$

We have two special cases:

1) Perfect match $(\square_{\mu}^{\nu} = \emptyset)$

$$A_{\mu}/A_{\emptyset} = \xi_{\nu}^{\mu}/\sqrt{\mu!} \qquad (22)$$

2) Perfect alignment $(\xi_{\nu} = \emptyset)$

$$A_{2\mu}/A_{\emptyset} = \left[(-1/2)^{\mu} \sqrt{2\mu!}/\mu!\right] \square_{\nu}^{2\mu}$$

$$A_{2\mu+1}/A_{\emptyset} = \emptyset \qquad (23)$$

where approximations have been used to obtain the results. Notice that mismatch only will produce purely even-indexed H-G (Hermite-Gaussian) modes.

Location of Hermite-Gaussian Modes in the Frequency Spectrum

The frequency of a $TEM_{m,n,q}$ mode is given by (Bilger, 1985b): $f_{mnq} =$

$$c/L\left[q + \frac{2}{\pi}(m+1/2)\cos^{-1}\left(1-\frac{L}{2\sqrt{2R}}\right) + \frac{2}{\pi}(n+1/2)\cos^{-1}\left(1-\frac{L}{4\sqrt{2R}}\right)\right] \quad (24)$$

where L is the resonator round-trip length, and R is the mirror radius of curvature (assumed the same for all four mirrors).

To identify the order of a particular mode, we can use the difference $f_{0,0,q+1} - f_{0,0,q} = c/L$ to give us the frequency difference between two successive longitudinal modes. The ratio $(f_{m,n,q} - f_{0,0,q}) / (f_{0,0,q+1} - f_{0,0,q})$ then gives the location of the m,n,-order mode in terms of this unit.

Thus,to identify a mode from the frequency spectrum, we measure its distance from the 0,0,q mode and divide this distance by the distance between the 0,0,q+1 and the 0,0,q modes. The result should be equal to the frequency ratio for a certain m and n.

We proceed to locate some of the more prominent high-order modes for the ring resonator:

The total length of the ring, L = 15.35 + 15.20 + 15.7 + 15.50 = 61.75 cm; there are four mirrors with diagonals approximately 45° to side of ring. The radius of curvature,

R is taken to be 5 m for all mirrors (see Chapter 3). The free spectral range (FSR) is given by:

FSR = c/L = 486 MHz

The frequency difference between a m,n,q mode and a Ø,Ø,q mode is given from Equation 24 by: $f_{m,n,q} - f_{Ø,Ø,q} = c/L$ (Ø.189m + Ø.133n)

TABLE I

LOCATION IN FREQUENCY OF SOME OF THE HIGHER-ORDER MODES

Mode	Freq. diff. (MHz)	Freq. ratio
ØØ	ØØ.Ø	Ø.ØØØ
Ø1	64.6	Ø.133
1Ø	91.8	Ø.189
11	156	Ø.322
2Ø	184	Ø.378
Ø2	129	Ø.266
21	248	Ø.511
12	221	Ø.455
22	313	Ø.644

All higher-order modes until and including m=3, n=3 are contained within Ø,Ø,q and Ø,Ø,q+1 .

Source Spatial Variation

Matching of the source beam with the resonator's eigenmode was satisfactorily done for a compromise ring waist size between the x and the y waists. The error in

matching was calculated to be < 11% implying a loss of only 1% of power into modes other than the fundamental Gaussian.

Since misalignment is a much more serious matter, and is prone to cause greater losses, a study was done to determine if there was excessive movement of the source beam both in tilt and offset due to say, changes in mirror positions inside the laser cavity. A large amount of movement could excite the ring resonator to oscillate in higher-order modes.

The lab setup for measurement of tilt and for measurement of offset were much the same (see Figure 18). Offset was determined by measuring the power spilling over a straight edge held close to the laser (3.5 cm from the front end). The edge was adjusted to block about 1/2 the power emitted by the laser. Any offset of the source beam would cause less or more power to spill over the edge. Since the spot size of the beam at the edge is known, the power measured can be expressed in terms of offset using formulae explained in the knife-edge scanning paper (Bilger and Habib, 1984). Any tilt of the beam would also result in a movement of the spot at the edge, but to a smaller degree than a pure offset of the same order since the edge is held close to the laser.

Spot size at detector (6 cm from laser waist) = 332 um

The spilled-over power is determined by the complementary error function (Q-function, Abramowitz, 1965), for which we use the following approximation:

$$Q(x) = 1/(1 + \exp[f(x)]) \; ; \quad f(x) = 1.5957x + .07295x^3 \qquad (25)$$

The power detected is given by :

$$P(x) = P_o \, Q[2(x-x_o)/322 \text{ um}] = P_o \, Q[2x/322 \text{ um}]$$

assuming $x_o = 0$ for $P(x) = 1/2$ Po as our reference point.

A movement of the beam relative to the straight edge can be considered as the edge moving relative to a stationary beam.

The beam offset which would cause changes in power around $P(x) = 1/2$ Po is calculated for two cases:

$P(x) = 0.49Po$	$x = -4.2$ um
$P(x) = 0.50Po$	$x = 0.0$ um
$P(x) = 0.51Po$	$x = +4.2$ um

Since the curve for the Q-function is linear around $P(x) = 1/2$ Po it is safe to extrapolate on a linear scale from $P(x) = 0.55Po$ to $P(x) = 0.45Po$.

As can be seen from Figure 23, the beam offset is much less than 5 um; it is of the order of 1/2 um. This apparent offset fluctuation could easily be caused by variation of laser beam power which is of the same order:

Laser power variation = 0.7 uW RMS

Power variation at straight edge = 1 uW RMS

It is interesting to calculate a tilt that would cause the same effect:

$$\alpha = \tan^{-1}(0.5\text{x}10^{-6}/6\text{x}10^{-2}) = 8.33\text{x}10^{-6} \text{ rad} \quad (\sim 1.7 \text{ arcsec})$$

Variation in tilt was measured by placing the straight edge 116 cm away from the waist of the laser, and performing the same set of measurements. Calculations are as follows:

Spot size 116 cm from waist = 786 um

P(x) = Po Q[2x/786um]

P(x) = Ø.49Po x = -9.8 um

P(x) = Ø.5ØPo x = Ø.Ø um

P(x) = Ø.51Po x = +9.8 um

A 9.8 um spot movement would indicate an angular wobble of :

$\alpha = \tan^{-1}(9.8x10^{-6}/1.16) = 8.5x1^{-6}$ rad (~1.7 arcsec)

Angular wobbles to a maximum of 1.5 arcsec were measured as is shown in Figure 24.

Both horizontal and vertical tilts were measured; horizontal offset was found to be quite the same as for vertical offset variations.

Since offsets or power variations would not account for more than Ø.5 um of spot movement, and spot movements of about 8 um were observed during tilt measurement, it is assumed that there is an angular beam wobble from the source laser. It is observed in (Fredricks, 1978, page 5Ø) that typical HeNe lasers have a beam wobble (tilt) of $3X10^{-5}$ rad (~6.2 arcsec).

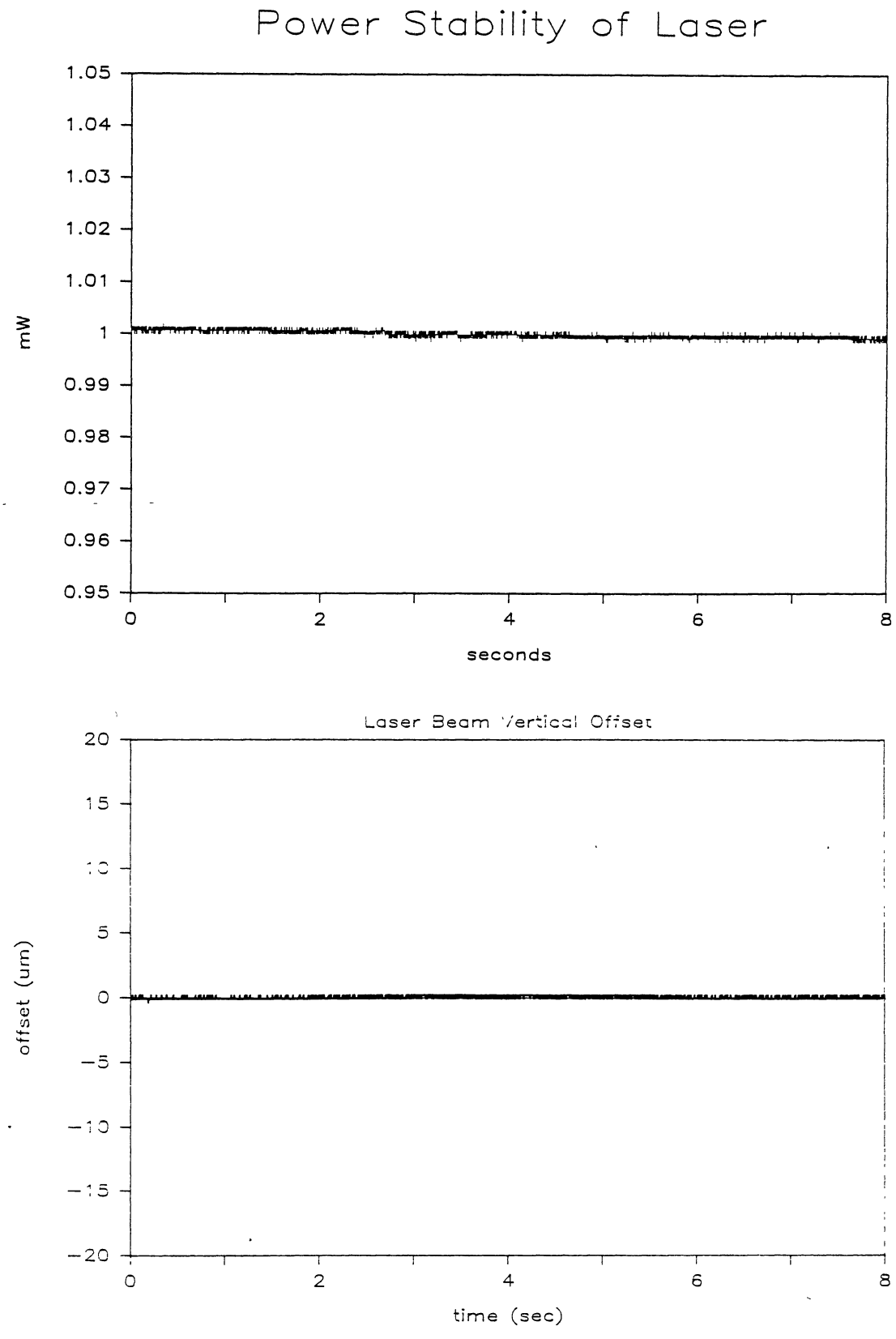

Figure 23. Comparison of power fluctuation vs vertical beam offset variation.

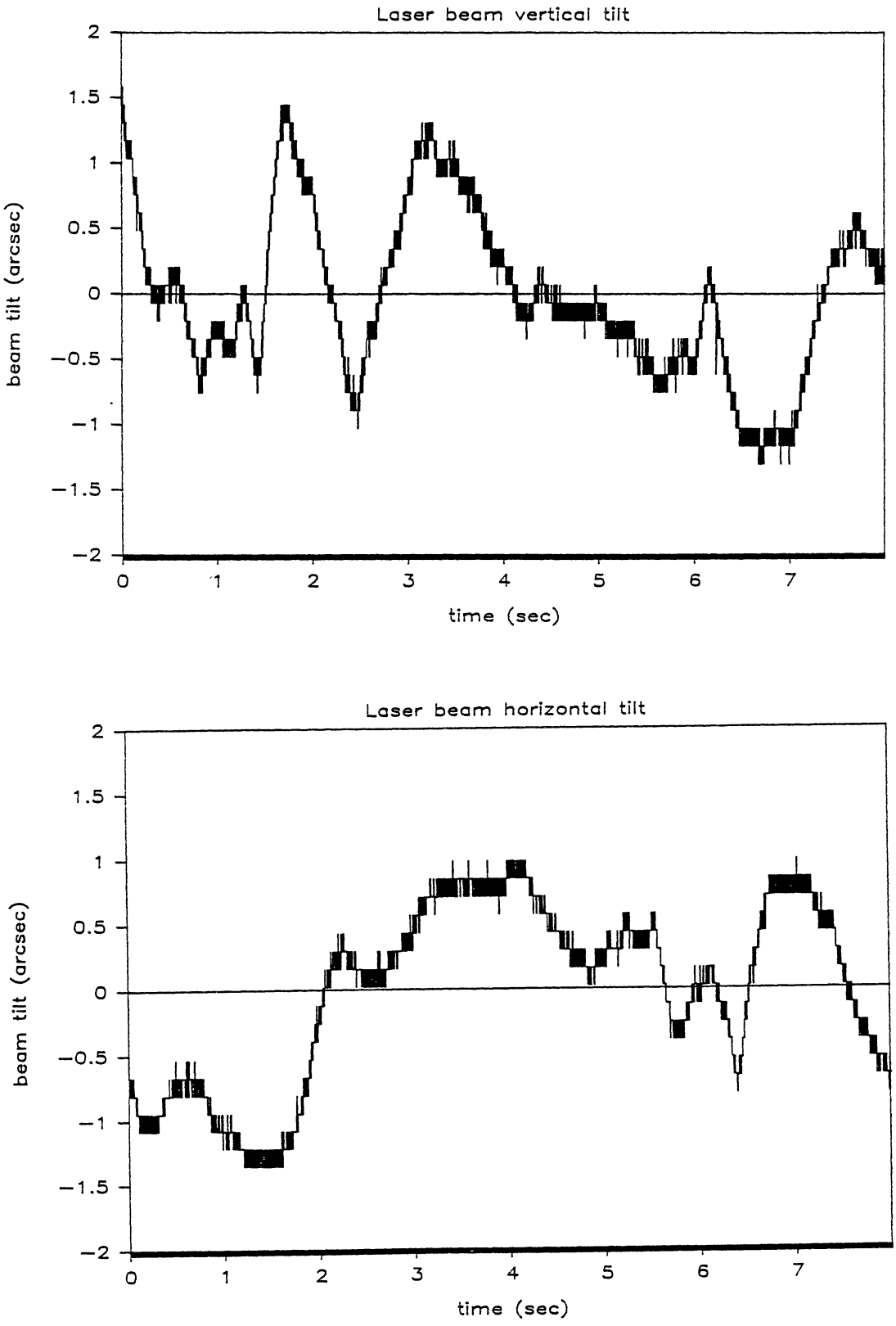

Figure 24. Vertical and horizontal beam tilt variation.

Generation of Higher-Order Modes in the Resonator

To get an idea of how the beam wobble would affect excitation of the ring, a comparison was made of the maximum angular tilt vs beam divergence, which are the units of measurement for the misalignment parameter. Beam divergence is given by:

$$w(z) \sim \frac{\lambda z}{\pi w_o} \quad ; \quad \frac{w(z)}{z} = \tan\Phi \sim \Phi$$

$$= \frac{\lambda}{\pi w_o} = \frac{633\times10^{-9}}{350\times10^{-6}} = 5.8\times10^{-4} \text{ rad} \quad \sim 120 \text{ arcsec}$$

This angle is of a much higher value than the beam wobble, which means that a beam tilt < 2 arcsec could be considered as a very minor error and would not cause any appreciable loss of power into the fundamental Gaussian.

A calculation is presented for the amplitude of a 1,0 mode caused by an angular movement of 8.5×10^{-6} rad in the xz-plane (we assume no offset error and no mismatch error). The mismatch parameter is given by:

$$\xi_x = \frac{(\varepsilon_x - q_{rx}\alpha_x)}{w_{rx}} = 0 + \frac{j\pi w_{rx}}{\lambda w_{rx}} 8.5\times10^{-2} = 0.014$$

For alignment, and proper match, the power ratio is given by:

$$\left|\frac{A_1}{A_0}\right|^2 = \left|\xi_x^{\,1}/_{\sqrt{1!}}\right|^2 = \left|\xi_x\right|^2 = 0.000196$$

Therefore the most prominent Hermite-Gaussian mode i.e. the 1,Ø mode will have only Ø.Ø2% of the amount of power present in the fundamental Gaussian, for this kind of beam tilt into the ring resonator.

The conclusion is therefore that the source is spatially stable enough to be used for excitation of the ring resonator.

CHAPTER VI

INTERNAL STABILITY

Analysis of Changes to the Optical Axis due to Mirror Rearrangements

A study of the internal geometric stability of the resonator was done to determine the new location of the optical axis due to mirror perturbations.

By definition, the eigenmodes of the ring resonator follow the path of the optical axis (eigenpath). However, the eigenmodes, which are a manifestation of the distribution of electric and magnetic fields inside the resonator, need not be considered to determine the change in the optical axis due to changes in mirror positions and tilts. Simple ray-tracing (Siegmann, 1971) provides a much simpler way to locate the new optical axis, and the eigenmodes will then be centered around the eigenpath.

That a new optical axis (relative to the old one, and consequently relative to the injecting source) can cause changes in the ring's output may be viewed in two cases.

1) Changes in tilt and offset of the injecting beam.

With reference to the new optical axis, the injecting source, which we assume was formerly perfectly aligned, may

now be injecting with a finite offset and tilt (see Figures 27 and 28); this may excite higher-order modes as explained in Chapter 5.

2) Changes in internal path length.

It is assumed that the ring was formerly 'tuned' with the injecting source i.e. the length of the optical axis is an integer times the wavelength of the injecting source (this may be done in ways outlined in Chapter 7). A change in the optical axis would cause a change in its total path length, relative to the old one. The source laser may now not be injecting into the frequency of the ring's fundamental Gaussian, but at the frequency of a higher-order mode (i.e. new length = integer x wavelength of higher-order mode). Along with the error in offset and tilt, that this could generate a purely higher-order mode is not very clear, however it would cause the ring's fundamental to be detuned with respect to the source. Note that it was observed when studying the ring output, that sometimes a fundamental mode would appear, and it intensity would slowly decrease.

It is assumed, of course in the above two cases that the beam is still contained within the confines of the resonator, and does not stray off the mirrors.

We undertake a brief study to examine how much power can be transferred into the higher-order modes in cases of extreme misalignment:

The power transfer into the resonator's Gaussian is given by (Sayeh, 1985)

$$P_{00}/P_L = \left|\equiv_x\right|^2 \left|\equiv_y\right|^2 = \exp\left[-\left|\xi_x\right|^2 - \left|\xi_y\right|^2 \right] \qquad (26)$$

for perfect match ($\alpha_\upsilon = 0$) , where

P_{oo} is the power present in the Ø,Ø mode,

P_L is the power in the source beam.

We examine misalignment along the x-axis only, so we can assume $\xi_y \ll \xi_x$

Then, $$P_{00}/P_L = \exp\left[-\left|\xi_x\right|^2 \right] \qquad (27)$$

Note that for large values of ξ_x (the misalignment parameter) very little power is transferred in the fundamental mode. The rest of the power injected into the resonator has to distribute itself amongst the higher-order modes.

To find the power present in any of the higher-order modes, we use the results from chapter five where the amplitude ratio of a higher-order mode to the fundamental Gaussian is given by:

$$A_{\mu/A_0} = \xi_\upsilon^{\mu} / \sqrt{\mu!} \qquad \text{for a perfect match.}$$

The power ratio of any higher-order to the zero order mode is $\left|A_{\mu/A_0}\right|^2$. For the 1,Ø mode or the Ø,1 mode,

$$\left|A_{\mu/A_0}\right|^2 = \left|\xi_\upsilon\right|^2 = \xi_\upsilon \xi_\upsilon^{*} \qquad (\upsilon = x \text{ or } y)$$

$$P_{10}/P_{00} = \left| \frac{\varepsilon_\upsilon}{w_{r\upsilon}} - j\frac{\pi}{\lambda}\frac{w_L^2}{w_{r\upsilon}}\alpha_\upsilon \right|^2 = \frac{\varepsilon_\upsilon^2}{w_{r\upsilon}^2} + \frac{\pi^2}{\lambda^2}\frac{w_L^4}{w_{r\upsilon}^2}\alpha_\upsilon^2 \qquad (28)$$

The power ratio can be made as large as possible by increasing ε_y (offset) or α_y (tilt).

To get an idea of the power transferred for this ring, we do a brief calculation in the x-plane for no offset ($\varepsilon_x = 0$), and a finite tilt.

$$P_{10}/P_{00} = \left|\xi_x\right|^2 = \frac{\pi^2}{\lambda^2}\frac{w_L^4}{w_{rx}^2}\alpha_x^2 = 2.72\times10^6\,\alpha_x^2$$

If the power in the 1,0 mode is to be 0.9 times as large as the power present in the 0,0 mode, $\alpha_x = 5.76\times10^{-4}$ rad (~120 arcsec). With this same type of error, the power ratio of the 2,0 mode to the 0,0 mode is:

$$P_{20}/P_{00} = \left|\xi_x^2/\sqrt{2}\right|^2 = \frac{\pi^4}{2\lambda^4}\frac{w_L^8}{w_{rx}^4}\alpha_x^4 = 0.9^2/2 = 0.4050$$

The total power transferred into the fundamental mode by the source is from Equation 27:

$$P_{00}/P_L = \exp\left[-\left|\xi_x\right|^2\right] = e^{0.9} = 0.4066$$

A table on the next page shows the percent power from the source injected into each of the orthogonal Hermite-Gaussian modes for the above example.

Since there is no mismatch and no misalignment in the y-plane, the m,0 modes are the only ones present, and the first 5 higher-order modes plus the fundamental mode contain almost all the power injected into the system.

TABLE II

PERCENT POWER PRESENT IN HIGHER-ORDER MODES DUE TO MISALIGNMENT IN THE X-PLANE

Mode	% Power Present
Ø,Ø	4Ø.66
1,Ø	36.59
2,Ø	16.47
3,Ø	4.94
4,Ø	1.11
5,Ø	Ø.2Ø
Sum	99.97%

For our ring mirror-error analysis, five types of mirror movements are possible.

x - translation — in the plane of the ring, perpendicular to the optical axis.

y - translation — in a plane perpendicular to that of the ring and perpendicular to the optical axis.

z - translation — in the plane of the ring and parallel to the optical axis.

theta - tilt — in a plane perpendicular to that of the optical axis.

phi - tilt — in a plane parallel to that of the optical axis.

To simplify matters, only one translation and one tilt, both in the plane of the ring will be investigated. It is assumed that all other mirror perturbations will have similar effects.

It is not evident how the new optical path could be determined analytically, although some recent research shows this is possible (Stedman, 1986). Computer simulation of the ring was done using ray matrices; help was gained from a previously done report (Habib, 1984). A short description of ray-matrices follows:

If a beam is injected with an input vector: offset α and tilt δ , the new offset α' and tilt δ' can be found both for traversal through a distance S, and a mirror with effective focal length f;

$$\begin{bmatrix} \delta' \\ \alpha' \end{bmatrix} = \begin{bmatrix} 1 & S \\ 0 & 1 \end{bmatrix} \begin{bmatrix} \delta \\ \alpha \end{bmatrix}$$

output vector — distance S — input vector

$$\begin{bmatrix} \delta' \\ \alpha' \end{bmatrix} = \begin{bmatrix} 1 & 0 \\ -1/f & 1 \end{bmatrix} \begin{bmatrix} \delta \\ \alpha \end{bmatrix}$$

output vector — mirror f — input vector

The system matrices are similar to those for transformation of q (Chapter 2).

The mirror perturbations cannot be expressed in matrix form in the same way, but have to be effected by an operation on the offset or tilt directly; following is the way they were implemented; both these perturbations were done on the mirror diagonally opposite the input mirror.

1) z - translation

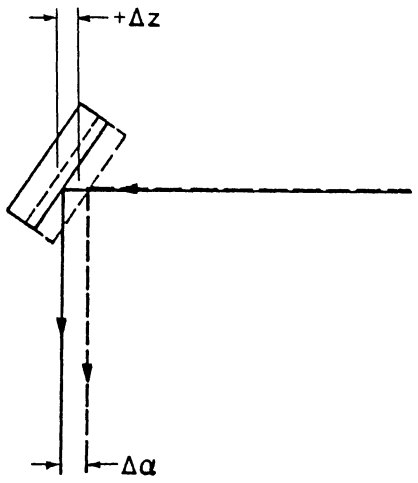

Figure 25. Effect on incoming ray if mirror translates by an amount Δ_z. Note that we are not assuming a closed-path here.

A translation of the mirror by an amount Δ_z directly offsets the beam by the same amount; this is of course a paraxial approximation assuming the beam still strikes the center of the mirror. The change in the ray vector is thus:

$$\begin{bmatrix} \delta' \\ \alpha' \end{bmatrix} = \begin{bmatrix} \delta+\Delta z \\ \alpha \end{bmatrix}$$

This change takes place after the ray hits the mirror.

2) <u>phi - tilt</u>

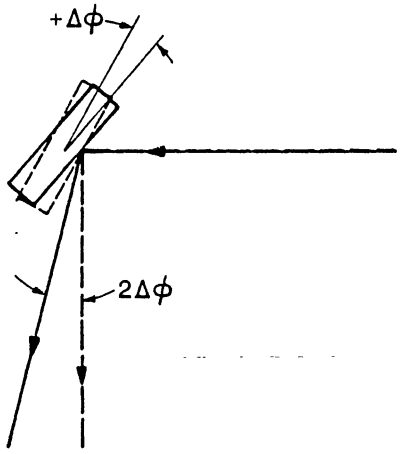

Figure 26. Effect on incoming ray if mirror tilts by an amount $\Delta\phi$. Note that we are not assuming a closed-path here.

A tilt of the mirror by an amount Δ_ϕ changes the output angle by twice that amount; Offset is not changed. The change in the ray vector is given by:

$$\begin{bmatrix} \delta' \\ \alpha' \end{bmatrix} = \begin{bmatrix} \delta \\ \alpha+2\Delta\phi \end{bmatrix}$$

This change is again effected after the beam strikes the mirror.

The computer algorithm to find the new optical axis worked in the following way:

1) Inject a ray vector into the system (four mirrors, a distance S apart, with a mirror perturbation) along the old optical axis; $\delta = \emptyset$, $\alpha = \emptyset$, and find the new output ray vector.

2) Inject a ray into the system with a offset halfway between the old and the new offset, and a tilt halfway between the old and the new tilt; find the new output ray vector and repeat the procedure till the injected and output ray vectors are the same. This would imply that the ray always followed the same (closed) eigenpath.

For the above types of mirror perturbations, it was found that convergence could be reached by using this method in all cases except when the mirrors were flat.
For mirrors with a large radius of curvature, the number of iterations for convergence was found to be very large; about 1ØØ iterations were required for a result good to 3 digits

for 5 m mirrors. Results are presented below for a square ring .16 m in length, with four 5 m mirrors.

z-translation; $= 1x10^{-6}$ m (1 um). After convergence,

delta = $1.34x10^{-6}$ m

alpha = $-1.67x10^{-5}$ rad

New path length = old path length + $3.9x10^{-6}$ m

(see Figure 27)

phi-tilt; $= 1x10^{-6}$ rad (Ø.2 arcsec). After convergence

delta = $9.43x10^{-6}$ m

alpha = $-2.68x10^{-6}$ rad

New path length = old path length + $9.5x10^{-6}$ m

(see Figure 28)

where delta and alpha represent the offsets and tilts that would repeat in one round trip i.e. define a closed path.

Figures 27 and 28 show the effects of the two types of mirror perturbations on the optical axis; the movements are grossly exaggerated for clarity.

It was noted that changes in path length, and tilts and offsets were of the same order as the perturbations themselves. The way these changes would affect the rings output is presented next.

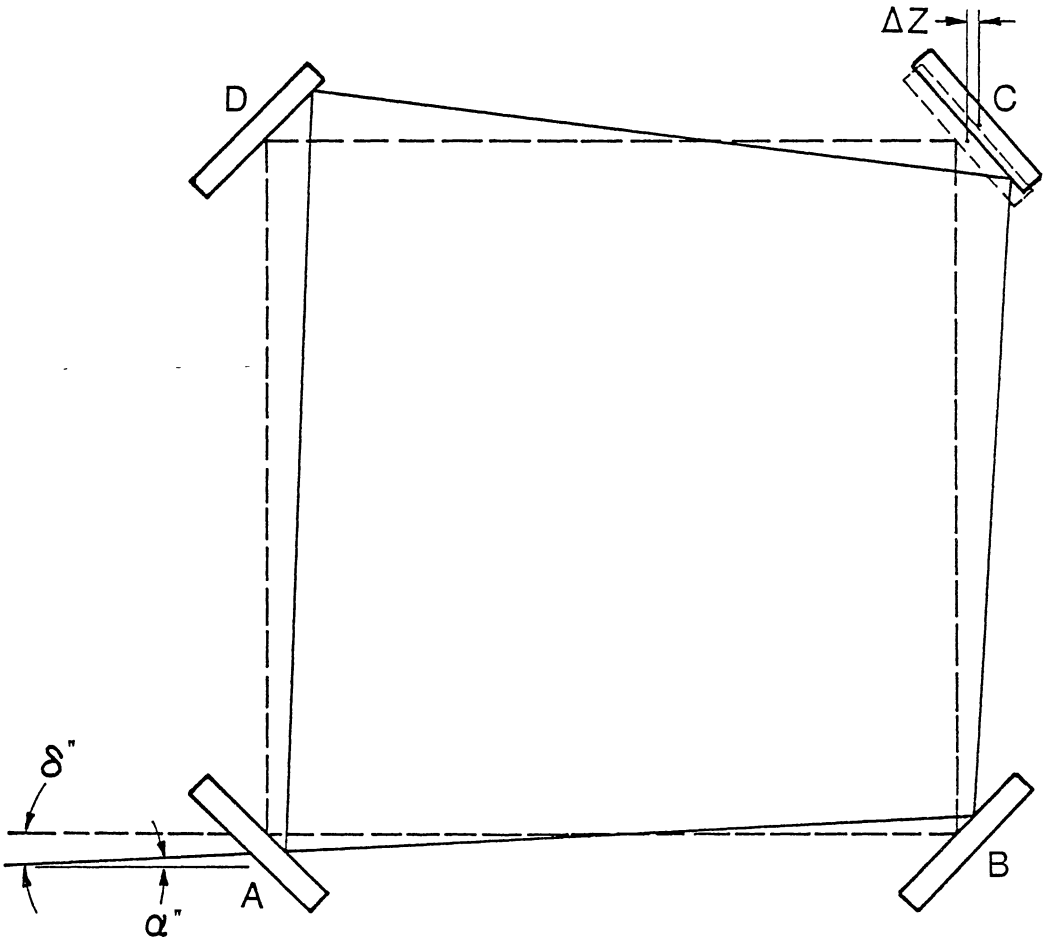

Figure 27 New closed-path resulting from a shift of Δ_z on mirror C; the tilt and offset of the new path relative to the old one is of the same order as the mirror perturbation.

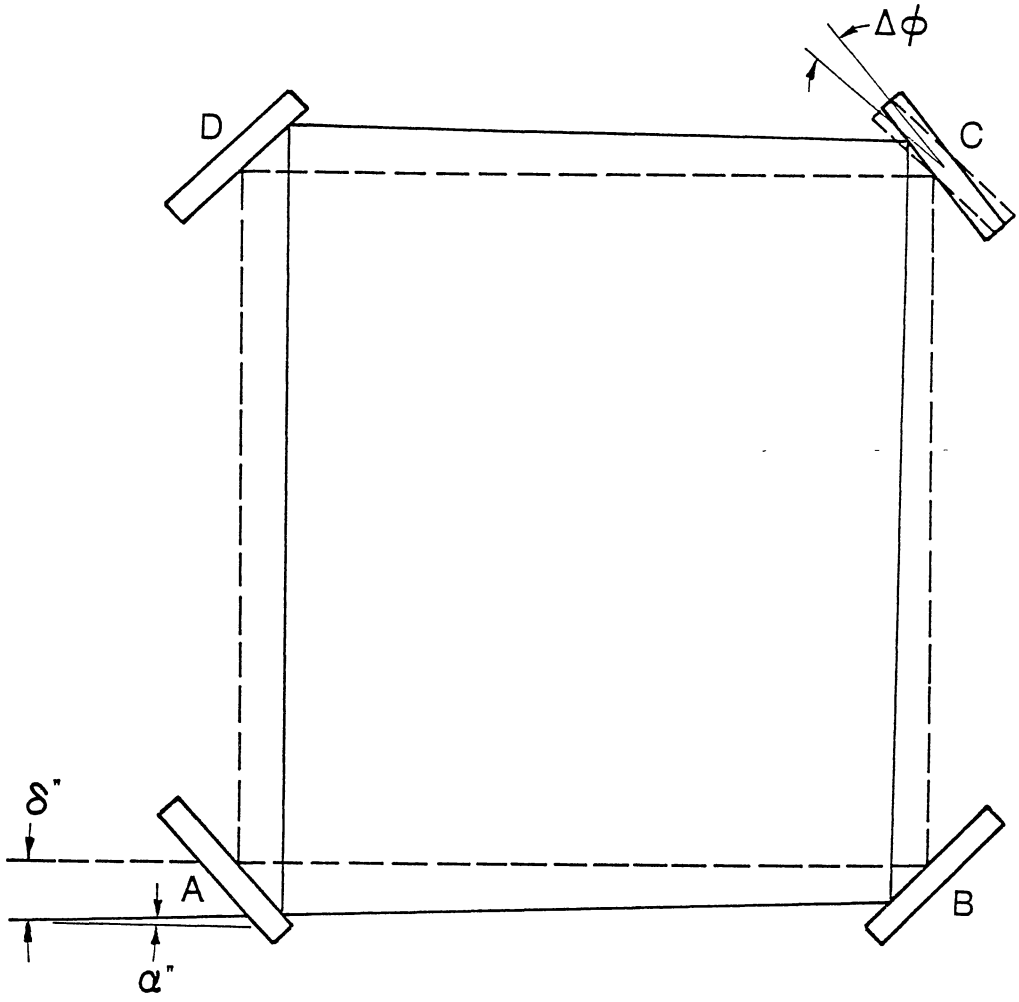

Figure 28 New closed-path resulting from a tilt of Δ_Φ on mirror C; the tilt and offset of the new path relative to the old one is of the same order as the mirror perturbation. Note however that the path-length change is appreciable compared to the wavelength of the source.

Excitation of Higher-Order Modes due to new Tilt and Offset

A change in the tilt and offset of the ring's optical axis relative to the source can be viewed as the ring's axis being stationary and the source now injecting with a new tilt and offset.

The value of the mismatch parameter from the new input vector due to the z-translation is derived below:

$\varepsilon_{H} = \delta = 1.34 \times 10^{-6}$

$\alpha_{H} = \alpha = -1.67 \times 10^{-5}$

$\xi_{H} = 4.09 \times 10^{-3} + j2.72 \times 10^{-2}$

$|\xi_{H}|^2 = 0.0076$

Assuming no mismatch, this is also the power ratio of the 1,0 mode to that of the fundamental Gaussian.

For phi-tilt of the mirror;

$\xi_{H} = 2.88 \times 10^{-2} + j4.36 \times 10^{-3}$

$|\xi_{H}|^2 = 0.00085$

Both of the above values for the misalignment parameter are too small to cause by themselves the output to change as drastically as was experimentally observed.

Change in Eigenfrequencies due to Path Length Variation

Resonance frequencies for the various modes for this particular ring is given in Chapter 5, Equation 24:

$$f_{mnq} = c/\text{Ø}.6175 \; (\; q + \text{Ø}.189m + \text{Ø}.133n + \text{Ø}.161 \;)$$

where q is an integer representing the longitudinal mode. We have:

freq. of the 1,Ø mode = freq. of Ø,Ø mode + 91.8 MHz

A frequency shift of 91.8 MHz could be caused by a ring length change calculated below:

Frequency of a fundamental mode is given by:

$$f_{\text{Ø},\text{Ø},q}' = (q+\text{Ø}.161)c/L$$

frequency of a 1,Ø mode after a length change is given by:

$$f_{1,\text{Ø},q} = (q+\text{Ø}.133+\text{Ø}.16)c/(L+dL)$$

Since the injecting frequency remains the same, the increase in length of dL shifts the eigenfrequencies of the ring relative to the source so that $f_{\text{Ø},\text{Ø},q}' = f_{1,\text{Ø},q}$

$$(q+\text{Ø}.161)c/L = (q+\text{Ø}.133+\text{Ø}.161)c/(L+dL)$$

After substituting $q = L/\lambda$ we get:

$$dL = \text{Ø}.133L/(L/\lambda+\text{Ø}.161) \sim \text{Ø}.133 = \text{Ø}.\text{Ø}8 \text{ um}$$

Which means that a length change of Ø.1 um in the eigenpath would cause a shift in the resonance frequency of ~92 MHz.

If the source laser was injecting at a fixed frequency of the fundamental Gaussian of the ring, this increase in optical path length would mean it was now injecting at a frequency of one of the 1,Ø modes. The previous results show that a eigenpath length change of Ø.1 um is well within the changes resulting for mirror perturbations of Δ_z = 1 um or Δ_ϕ= Ø.2 arcsec.

Path length changes of this order may also be caused by changes in refractive index of the medium enclosing the beam path. An expression for variation in refractive index of air vs temperature change is given by (Kaye, 1973, page 86):

$$n_{tp}-1 = (n_s-1)\frac{p[1+p(61.3-t)10^{-10}]}{9600 95.4(1+0.00366 1t)} \qquad (29)$$

where n_{tp} = refractive index at temperature t and pressure p

n_s = refractive index at 15°C and 101325 Pa

t is given in °C, and p in Pa (N/m^2)

The difference between the refractive index at 15°C and that at 15.1°C is of the order of $1x10^{-7}$, and this would directly correspond to a path length change of the same order (.1 um)

It therefore stands to reason that the beam-path should be contained in vacuum, or in a medium with a lesser refractive index than that of air (helium for example).

Comparison with Practical Effects

The question now is if mirror rearrangements of the order investigated are likely to take place in the ring resonator constructed.

The coefficient of thermal expansion of granite is given as $\sim 8 \times 10^{-6}\ K^{-1}$ (Creswell, 1966) which means that a change in the temperature of the table surface by $1/10\ ^{\circ}C$ could cause a mirror to shift (translate) by 1 um. A change of $1/100\ ^{\circ}C$ would then be able to cause a frequency shift into one of the higher modes, for this particular ring constructed on a granite base.

A mirror tilt of 0.2 arcsec sounds like a very possible effect. The holders or mirrors themselves might tilt due to thermal changes or vibrations. In fact, it was found that the output of the ring could be greatly disturbed by thumping on the floor some distance from the setup; vibration frequencies caused by the thumping could be detected in the output of the ring.

Changes in refractive index of the surrounding medium could also cause appreciable path length changes although this would be a relatively slow effect compared to the previously mentioned factors, if it had to occur over the entire path length.

CHAPTER VII

CONCLUSIONS AND RECOMMENDATIONS

Summary and Conclusions

A reasonably square ring resonator with length Ø.154 m on a side was constructed in the laboratory from 5 m radii mirrors. A source was matched and aligned with the optical axis of the resonator, and after adjustments, a continuous series of short-lived resonances was observed. A visual study of the output showed the apparent presence of higher-order modes as well as the fundamental Gaussian; these modes were found to be unstable and would decay in intensity or change into other modes.

Analysis from the last two chapters suggest that the source is not responsible for the instability of the ring output. The relatively slow decay in the intensity of the modes may be due to thermally-induced length changes in the ring; the rapid change from one mode to another could be caused by 'mirror noise' - the holders or mirrors tilting due to low-frequency vibrations carried through to the table and causing abrupt length changes.

Tilt of offset of the source beam against the resonator's optical axis is a relatively minor source of error compared to effects caused by changes in internal

geometry of the ring, or changes in refractive index of the medium surrounding the beam-path.

Recommendations

The following suggestions are given to anyone intending to build a passive ring-resonator in the laboratory.

1) The ring should be mounted on a surface with a very low coefficient of thermal-expansion, for example, Zeroduer, or even invar; then temperature fluctuations of the environment in tenths of degrees can be tolerated.

2) Mirror-holders should be rigid and have locks on the adjustments (i.e. screws which would rigidly fix the mirrors once positioning was obtained).

3) Mirrors should be used which have a high reflectivity at incident angles that would be encountered in the resonator.

4) Mounting for the ring should be vibrationally isolated from the rest of the lab environment.

5) Fine-tuning of the resonator for maximum transmission of a mode could be accomplished by slightly tilting the mirrors (Bilger, 1986); as previously shown, the misadjustment caused by this would be far less than the change in path-length which accomplishes the fine-tuning.

Once maximum transmission is obtained, the mirrors should be locked into position.

6) It would be wise to enclose the beam path with a set of quartz tubes, or to evacuate the path entirely. This would eliminate drag-effects caused by moving masses of air, or variation in path length caused by changes in refractive index of the surrounding medium.

7) A stabilized source (in frequency, space and intensity) is very necessary.

The practical application to this study is of course, not just to build a ring resonator, but to construct a Passive Ring Laser Gyro (PRLG), which has two counter-propagating beams following the same eigenpath. The gyro has several applications including the measurement of very small rotational rates.

SELECTED REFERENCES

Abramowitz, M., and Stegun, I. A., 1965, Handbook of Mathematical Functions, Dover.

Al'tshuler, G. B., et al., 1977, "Analysis of Misalignment Sensitivity of Ring-Laser Resonators", Sov. J. Quantum Electron., vol 7, 857, July 1977.

Baxter, T. D., Saito, T. T., et al., 1983, "Mode Matching for a Passive Resonant Ring Laser Gyroscope", Appl. Opt., vol. 22, 2487, 1983.

Bilger, H. R. and Habib, T., 1985 "Knife-edge Scanning of an Astigmatic Gaussian Beam", Appl. Opt., Vol 25, page 686, 1 March 1985.

Bilger, H. R., 1985b, Modelling a large ring resonator gyroscope, Publication for AFOSR grant No. 84-ØØ58, 3Ø Mar 1985.

Bilger, H. R., 1986, Private communication.

Born, M. and Wolf, E., 1983, Principles of Optics, Macmillan, New York, 1983.

Creswell, A. A., 1966, Structural Engineering Data Book, Pitmann.

Collins, S. A., 1964, "Analysis of Optical Resonators Involving Focusing Elements", Appl. Opt., vol.3, 1263, Nov 1964.

Ezekiel, S. and Balsamo, S. R., 1977, "Passive Ring Resonator Gyroscope", Appl. Phys. Lett., May 1977.

Fredricks, R. J. and Carrington, W. A., 1978, "Sources of Error in a Discrete Component Saganc Optical Rotation Rate Sensor", SPIE, Vol 157, Laser Inertial Rotation Sensors, 1978.

Habib, T., 1984, "Ray-tracing in an optical cavity", Oklahoma State University report submitted as part of course-work.

Haus, H. A., 1984, Waves and fields in optoelectronics, Prentice-Hall, 1984.

Heer, C. V., 1984, "History of the Laser Gyro", SPIE, vol 487, Physics of Optical Ring Gyros.

Rosenthal, A. H., 1962, "Regenerative circulatory multiple-beam interferometery for the study of light-propogation effects", J. Opt. Soc. Amer., vol 52, No 1Ø, Oct 1962.

Sayeh, M. R., Bilger, H. R. and Habib, T., 1985, "Optical resonator with an external source: excitation of the Hermite-Gaussian modes", Appl. Opt., 15 Nov. 1985.

Siegman, A. E., 1971, An Introduction to Lasers and Masers, McGraw-Hill, 1971.

Stedman, G. E., and Bilger, H. R., 1986, "Stability of planar ring lasers with mirror misalignment", To be submitted for publication

Stowell, W. K., 1974, "A Precision Measurement of Fresnel Drag in a Ring Laser", unpublished dissertation, Oklahoma State University.

Yamauchi, N., 1974, "Resonant modes in a Ring Laser Resonator and Their Deformation by Mirror Rearran gements", Electron. and Comm. in Japan, vol 57-C, No. 11.

Verdeyen, J. T., 1985, Laser Electronics, Prentice-Hall, 1985

APPENDIX A

EXPRESSIONS FOR THE FINESSE OF A RESONATOR AND ITS RELATION TO THE QUALITY FACTOR

The finesse of a resonator is defined from its resonance curve (Born, 1984, page 328) as the full width at half-maximum divided by the free spectral range, i.e. the ratio of the "width between the points in either side of a maximum where the intensity has fallen to half its maximum value" to the "separation of adjacent fringes". This may be directly measured from a resonance curve obtained by a frequency analyzer.

The finesse can also be calculated from the transmission intensity relationship for a four-mirror resonator. Equation 4 in Chapter three gives us the following:

$$I_o = \frac{k\ I_{in}}{(1 - R)^2 + 4R\sin^2(d/2)}$$

where $k = t_A^2 r_B^2 t_C^2$ and $R = r_A r_B r_C r_D$

$$I_o = \frac{k'\ I_{in}}{1 + Y\sin^2(d/2)} \qquad \text{for } Y = 4R/(1 - R)^2$$

The maximum output power is given by: $I_{max} = k'\ I_{in}$.
At a point where the intensity is half its maximum value,

$$\frac{1}{1 + Y\sin^2(d/2)} = \frac{1}{2}$$

at $d = 2m + \varepsilon/2$ for small values of ε, $\sin\varepsilon =$

$$\frac{1}{1 + Y^2/4^2} = \frac{1}{2}$$

and we have $\varepsilon = 4/(Y)^{1/2}$

In terms of frequency spacing from the resonance curve, the finesse is given by:

$$\text{finesse} = \frac{2\pi}{2(\varepsilon/2)} = \frac{\pi(Y)^{1/2}}{2}$$

substituting back the value for Y, we finally have:

$$\text{finesse} = \frac{\pi(R)^{1/2}}{(1 - R)}$$

The quality factor, Q of a cavity is given by the absolute frequency of resonance divided by the full-width at half maximum: $Q = f_o/\Delta f$.

The finesse can be written as :

$$F = \frac{(f_o + c/L) - (f_o)}{\Delta f} = \frac{c}{L\,\Delta f}$$

but $c = \lambda f_o$

$$F = \frac{\lambda f_o}{L\,\Delta f} = \frac{\lambda}{L}\,Q$$

Therefore, the quality factor is given by: $Q = L/\lambda\ F$

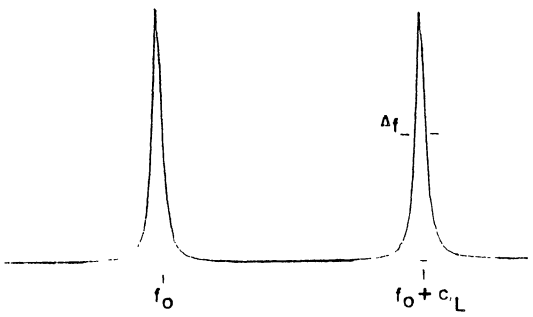

APPENDIX B

KNIFE-EDGE SCANNING OF AN ASTIGMATIC GAUSSIAN BEAM

Knife-edge scanning of an astigmatic Gaussian beam

Hans R. Bilger and Taufiq Habib

The relations for position, spot size, and inclination of the major axis of an elliptical Gaussian beam to knife-edge scanning data are derived. A knife-edge whose scanning direction is adjustable to any angle has been employed to scan across a beam in at least three directions. Nonlinear least-squares fit programs have been developed to check whether a beam is Gaussian, and to evaluate the parameters, with errors, of such an elliptic spot. The evolution of an astigmatic beam in the tangential and sagittal plane is measured

I. Introduction

Scanning of a Gaussian beam with circular cross section has been dealt with in several papers.[1] However, beams with different cross sections or power density distributions appear often in laser systems either as aberrations, e.g., through admixture of Hermite-Gaussian beams, or as an essential feature, as is the case in ring lasers. The extension reported here has several benefits in the laboratory:

(1) Quantitative determination of the degree to which a given spot deviates from a circular cross section.

(2) Determination of the parameters of an elliptical spot.

(3) Analytical (least-squares) evaluation of the spot, including an estimate of the errors of the evaluated parameters.

II. Scanning of a Gaussian Beam with Elliptical Cross Section

The spot size w shall be defined by the following distribution of the electric field amplitude E:

$$E(x,y) = E_0 \exp[-(x^2 + y^2)/w^2] \tag{1}$$

for a circular beam spot centered at $x = y = 0$; the beam propagates in the direction of the positive z axis.

Extending this to an elliptical cross section with arbitrary orientation (see Fig. 1) and using power density S (proportional to intensity I), we have

$$S(x',y') = \frac{2}{\pi}\frac{P_0}{w_a w_b} \exp(-2x'^2/w_a^2) \exp(-2y'^2/w_b^2), \tag{2}$$

where w_a, w_b are the spot sizes along the major and minor axes, respectively, P_0 is the total power in the beam, $2(P_0/\pi w_a w_b)$ is the power density in the beam center, and

$$\begin{aligned} x - x_0 &= x' \cos\alpha_0 - y' \sin\alpha_0, \\ y - y_0 &= x' \sin\alpha_0 + y' \cos\alpha_0. \end{aligned} \tag{3}$$

Equations (3) include rotation by a tilt angle α_0 (measured from the positive x axis in the direction of the positive y axis) and translation of the beam center to x_0, y_0. A centered circular Gaussian beam [Eq. (1)] is included as a special case with $x_0 = y_0 = 0$ and $w_a = w_b = w$.

When a straightedge is placed at $x = x_s$ parallel to the y axis, obscuring the half-plane $x \leq x_s$, the power transmitted past the edge[2] is given by

$$P(x_s) = \int_{x=x_s}^{x=+\infty} \left[\int_{y=-\infty}^{y=+\infty} S(x,y)dy\right] dx \tag{4}$$

This double integral can be expressed as a complementary error function of x_s,[3] namely,

$$P(x_s) = (P_0/2)\,\mathrm{erfc}(u), \qquad u = (\sqrt{2})(x_s - \bar{x}_s)/w(\alpha_0), \tag{5}$$

with $\mathrm{erfc}(u) = (2/\sqrt{\pi})\int_u^\infty \exp(-t^2)dt$, or as[4]

$$P(x_s)/P_0 = Q(v), \qquad v = [2/w(\alpha_0)](x_s - \bar{x}_s) = (\sqrt{2})u, \tag{6}$$

with

$$Q(v) = [1/\sqrt{(2\pi)}] \int_v^\infty \exp(-t^2/2)dt,$$

and

$$\begin{aligned} w^2(\alpha_0) &= w_a^2 \cos^2\alpha_0 + w_b^2 \sin^2\alpha_0, \\ \bar{x}_s(\alpha_0) &= x_0 \cos\alpha_0 + y_0 \sin\alpha_0 + x_{so} \end{aligned} \tag{7}$$

(x_{so} is the offset of the translator micrometer).

The function $P(x_s)/P_0$ is drawn in Fig. 2 vs scanner position x_s for two widths, w_1 and w_2; the center of the beam is assumed to be at $x_s = 0$. Equation (7) contains the three parameters of interest w_a, w_b, and α_0. The apparent width $w(\alpha_0)$ is plotted in a polar plot in Fig

The authors are with Oklahoma State University, School of Electrical & Computer Engineering, Stillwater, Oklahoma 74078.

Received 24 September 1984.
0003-6935/85/050686-05$02.00/0.

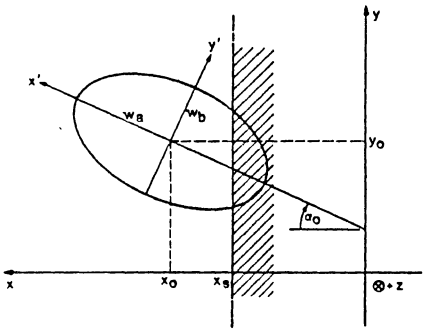

Fig. 1. Elliptical beam spot centered at x_0,y_0 with axes w_a and w_b tilted against the positive x axis (horizontal) by α_0. The beam goes into the paper plane (positive z axis). The scanning edge is placed at x_s.

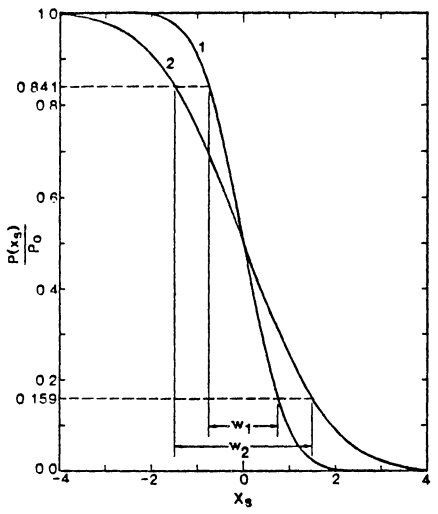

Fig. 2. Relative power $P(x_s)/P_0$ vs scanner position x_s for two spot sizes w_1 (= 1.5 units on the abscissa) and w_2 (= 3 units on the abscissa). The shapes of these curves are identical, except for a difference in w, for scanning of an arbitrarily placed elliptical beam. The beam centers are assumed to be at $x_s = 0$.

3 for three different ratios w_a/w_b, together with the actual spot shape (ellipse, dashed line) for $w_a/w_b = 2$. The measured widths $w(\alpha_0)$ agree with the widths of the ellipse at $\alpha = \alpha_0$ and $\alpha = \alpha_0 \pm 180°$ where $w(\alpha_0) = w_a$, and at $\alpha = \alpha_0 \pm 90°$ where $w(\alpha_0) = w_b$.

If the scanner is now rotated around the z axis by an angle α against the positive x axis, the equation for the resulting width is slightly generalized to

$$w^2(\alpha) = w_a^2 \cos^2(\alpha_0 - \alpha) + w_b^2 \sin^2(\alpha_0 - \alpha),$$
$$\bar{x}_s(\alpha) = x_0 \cos(\alpha_0 - \alpha) + y_0 \sin(\alpha_0 - \alpha) + x_s 0. \quad (8)$$

For a circular beam with $w_a = w_b = w$, the result is again $w(\alpha) = \text{const} = w$, as it should be.

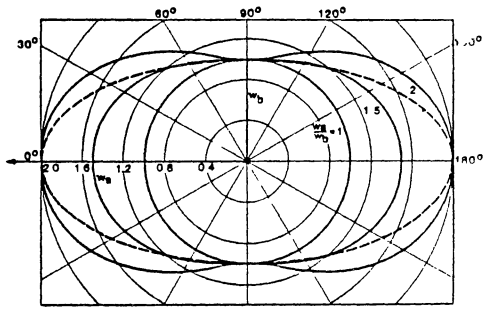

Fig. 3. Polar plot of widths vs scanning angle α for three different elliptical beam spots (solid curves). The spot for $w_a/w_b = 2$ is drawn as a dashed ellipse.

Three methods have been devised to evaluate $w(\alpha)$:

(a) Fractional power method: Noting that $Q(v_+ = 1) = 0.841 = P(x_s^+)/P_0$, and $Q(v_- = -1) = 0.159 = P(x_s^-)/P_0$ (see Fig. 2), we set the edge such that the relative power equals these fractions. The positions x_s^+ and x_s^- yield the width $w(\alpha)$ through

$$v_+ - v_- = 2 = [2/w(\alpha)](x_s^+ - \bar{x}_s) - [2/w(\alpha)](x_s^- - \bar{x}_s),$$

or

$$w(\alpha) = x_s^+ - x_s^- \quad (9)$$

In principle, any pair v_+v_- can be chosen to evaluate w, but with a given absolute error in $P(v)$, it can be shown that the pair $v_\pm = \pm 1$ produces the width with minimum relative error. The center of the beam, $\bar{x}_s$, can be obtained by setting the scanner such that the transmitted power is halved, see Fig. 2.

(b) Graphical method: This method consists of plotting the relative power $P(x_s)/P_0$ vs x_s on error function paper.[5] A straight line on this paper indicates an error function, i.e., that the beam is indeed Gaussian. The points x_s^+ and x_s^- can then be used as above to find w. The center of the beam is again given by $P(\bar{x}_s)/P_0 = 1/2$. This method has the advantage over method (a) in that it makes use of all the measured scanning positions, that the latter do not have to be specifically chosen, and that the graph allows a check whether the beam is Gaussian. It also provides some estimate of measurement errors.

(c) Least-squares method: This third method consists of fitting the Q-function into the measured power vs x_s (see Fig. 2), by adjusting the three parameters P_0, w, and $\bar{x}_s$. This method does not require the data to be normalized with the power P_0 before analysis. It can furthermore accommodate a fluctuating total power and it reduces errors introduced by fluctuating power. The accuracy of the computer program is not limited to the usual ~1% of graphical methods. Any observer bias is eliminated. Finally the program also provides analytic estimates of the errors of the parameters by calculating the variance-covariance matrix.[6]

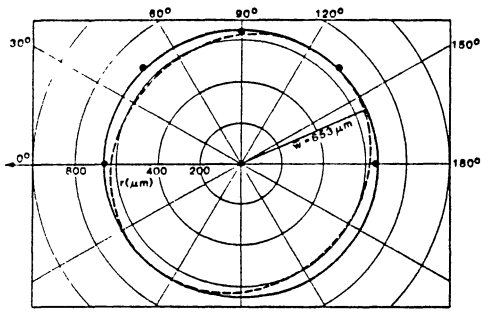

Fig. 4. Test of a spot at z = 90 cm off the laser without intervening optics at 5 angles, 0°, 45°, 90°, 135°, and 180°. The fit $w(\alpha)$ = const results in w = (653 ± 4) μm. The sensitivity of the method to detect ellipticity is demonstrated by the dashed curve where tentatively w_b/w_a = 0.9 has been set.

Given the measured points $P(x_s)$, usually between five and twenty points covering the range from 0.9 P_0 to 0.1 P_0, the program fits the function

$$P(x) = a_1 Q[2(x - a_3)/a_2] \tag{6a}$$

into the points where $a_1 = P_0$, $a_2 = w(\alpha)$, $a_3 = \bar{x}_s$. An approximation for Q is chosen[4] which has a maximum error of $\pm 1 \times 10^{-5}$ over all arguments v:

$$Q(v) \simeq \tfrac{1}{2} + \mathrm{sgn}(v)\{[1/\sqrt{(2\pi)}] \times (a + bt + ct^2)t \exp(-v^2/2) - 1/2\},$$

$$t = 1/(1 + p|v|),$$

$$\mathrm{sgn}(v < 0) = -1, \quad \mathrm{sgn}(v = 0) = 0, \quad \mathrm{sgn}(v > 0) = +1,$$

$$p = 0.33267, a = 0.4361836,$$

$$b = -0.1201676, c = 0.9372980.$$

The program is iterative. It makes use of initial estimates for a_1, a_2, a_3 and refines these estimates until the sum of the residuals squared is satisfactorily close to the minimum. For a set of twenty points, the program takes ~800-msec CPU time on the VAX 11/750 for four iterations, which usually leads to convergence.[7]

III. Parameters of a Gaussian Beam with Elliptical Cross Section

One scan at an angle α gives $w(\alpha) = a_2$. We need at least three scans to calculate w_a, w_b, and α_0. In practice, scans at more than three angles are made. A separate least-squares fit program then determines the three parameters above through Eq. (8) or through

$$w(\alpha) = w_a\sqrt{[1 - \epsilon^2 \sin^2(\alpha_0 - \alpha)]}, \tag{8a}$$

with ϵ = numerical eccentricity = $\sqrt{(1 - w_b^2/w_a^2)}$.

IV. Establishment of an astigmatic Gaussian beam

A He–Ne laser (Oriel model 6697) was used to produce a well-behaved circular Gaussian beam. Its circularity was checked by scanning at several angles, see Fig. 4. A silicon detector (Optics Technology model 610) with a narrowband optical interference filter was used for detection with background light. The beam evolution was measured within the first 1.5 m off the laser front end. The spot size vs z was fitted by the equation

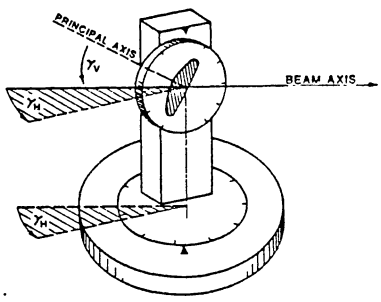

Fig. 5. Goniometer to adjust the obliquity angle of the lens The reference position is given by retroreflection which originally aligns the principal axis of the lens with the beam axis = optical axis

$$w(z) = w_0\sqrt{[1 + (z - z_w)^2/z_0^2]}, \tag{11}$$

with w_0 = waist size, located at $z = z_w$, and z_0 = Rayleigh length = $\pi w_0^2/\lambda$. The waist location z_w was found near the output mirror of the laser. The waist size was w_0 = (316 ± 5) μm.

A plano-convex lens with focal length f_0 = 20 cm was then placed on a rudimentary goniometer (Fig. 5), which enabled us to rotate the lens around a vertical axis by an angle λ_h and also around a horizontal axis by an angle λ_v. The angle of obliquity[8] ϕ between the beam and the principal axis of the lens then becomes

$$\phi = \arccos(\cos\gamma_h \cos\gamma_v). \tag{12}$$

This angle lies in the tangential plane whose tilt against the horizontal plane (x-z plane) is given by

$$\alpha_0 = \arcsin(\sin\gamma_v/\sin\phi). \tag{13}$$

The tangential plane therefore contains one of the axes of the ellipse.

The lens was placed at $2f_0$ = 40 cm from the beam waist, with the two angles $\gamma_h = \gamma_v \approx 30°$, which results in the two focal lengths[9]: $f_{\text{tangential}}$ = 9.4 cm and f_{sagittal} = 16.8 cm. The beam, after traversing the lens, is expected to have a shape as given in Fig. 6, with the circle of least confusion[8,9] at $z \approx 15.5$ cm; before and after this point, the ellipse rotates by −90° (α_0 = 136.5° to α_0 = 46.5°). Since the input to the lens is a circular Gaussian beam, there will be a tangential waist and a sagittal waist placed approximately symmetrical to $z_{l,c}$. There are no focal lines in this case.

The propagation of the beam in the tangential plane is independent of that in the sagittal plane. Both are governed by Eq. (11), with two different sets of parameters: w_{0t}, z_{wt}, z_{0t}, and w_{0s}, z_{ws}, z_{0s}.

V. Experimental Evaluation of the Astigmatic Beam

The beam was probed at distances 12–60 cm after the lens. This range contains the interesting features (see Fig. 6): primary focus = waist in the tangential plane,

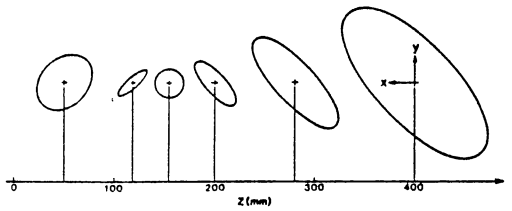

Fig 6. Evolution of beam along the z axis. The circular Gaussian beam enters the lens at $z = 0$. The spots are shown as they appear in the x-y plane enlarged by ×100 relative to the z scale. Immediately to the left and right of the circle of least confusion, the tangential and sagittal waists are shown, respectively.

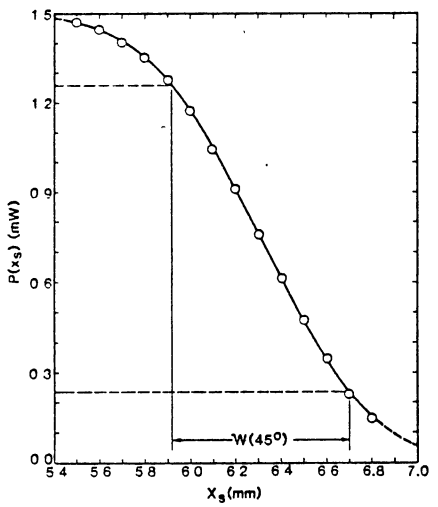

Fig 7. Scan of astigmatic beam at $z = 60$ cm from the lens at $\alpha = 45°$. The least-squares fitted parameters are: total power $P_0 = (1.498 \pm 0.005)$ mW, center at $\bar{x}_s = (6\,309 \pm 0.002)$ mm, spot size $w(45°) = (783 \pm 6)$ μm.

circle of least confusion, and secondary focus = waist in the sagittal plane.

Figure 7 shows a typical measurement of $P(x)$ at a distance $z = 60$ cm from the lens, at a scanning angle $\alpha = 45°$ with respect to the positive x axis. The least-squares fit of Eq. (6a) to the fourteen measured points gives $P_0 = (1.498 \pm 0.005)$ mW, $w(45°) = (783 \pm 6)$ μm, $\bar{x}_s = (6.309 \pm 0.002)$ mm. None of the individual residuals exceeded 8 μW; a translator with 10-μm resolution (smallest division) was used.

After at least four widths are evaluated for each spot, Eq. (8a) is fitted into the data $w(\alpha)$. Figure 8 shows a typical fit at $z = 35$ cm with the result $w_a = (801 \pm 3)$ μm, $\varepsilon = 0.920 \pm 0.003$, $\alpha_0 = (46.4 \pm 0.4)°$, which establishes the tilt and size of the ellipse at 35 cm together with the errors. The maximum deviation is 7.5 μm; the average deviation is 4 μm.

Finally, the evolution of the tangential spot sizes $w_t(z)$ and the sagittal spot sizes $w_s(z)$ is obtained (see

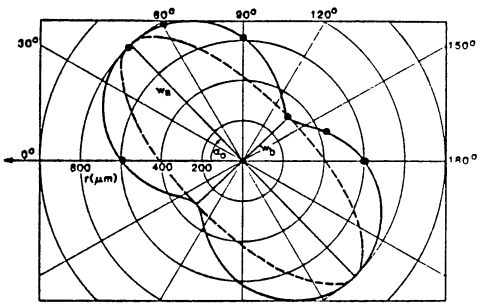

Fig. 8. Polar plot of spot sizes $w(\alpha)$, taken at $z = 35$ cm. The fit gives $w_a = (801 \pm 3)$ μm, $\varepsilon = 0.920 \pm 0.003$, $\alpha_0 = (46.4 \pm 0.4)°$. The rms deviation of the widths in this plot from the best-fitted solid curve is 4.5 μm. The resulting elliptical spot size is drawn as a dashed curve.

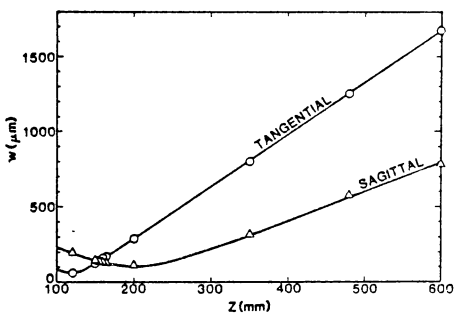

Fig. 9. Evolution of astigmatic beam vs z (see also Fig. 6). The waist sizes are $w_{0t} = (58.0 \pm 0.2)$ μm and $w_{0s} = (102.0 \pm 1.2)$ μm. They can be located with an accuracy of about ±2 mm.

Fig. 9) by least-square fitting Eq. (11) into the previously obtained results. The best-fitted parameters are

tangential waist $w_{0t} = (58.0 \pm 0.2)$ μm at $z_{wt} = (118.5 \pm 0.9)$ mm,

sagittal waist $w_{0s} = (102.0 \pm 1.2)$ μm at $z_{ws} = (201.3 \pm 2.5)$ mm.

The maximum deviation of any point was 8.5 μm for the tangential spot sizes and 14.6 μm for the sagittal spot sizes.

VI. Discussion of Results

The methods used here to scan an elliptical Gaussian beam with a straightedge (razor blade) are based on the result that the power spilling over the blade has the same dependence on the position of the blade as is the case in a circular Gaussian beam, except that the evaluated width is a simple function of position and size of the ellipse. At least three scans need to be done on each spot, with different angles α. If the position of the tangential plane (α_0) is known, two measurements would suffice, preferably taken at $\alpha = \alpha_0$ and $\alpha = \alpha_0 \pm 90°$.

Two methods were mainly used to obtain a width, namely, the fractional power method and the least-squares method. The latter established that the beam is indeed Gaussian, within the errors. However, subsequent measurements were usually done with the fractional power method, which is faster. Both methods yield typical errors of the order of one small division on the scanner (= 10 μm) or less. The data suggest indeed that translators with a resolution of 1 μm would produce yet smaller random errors.

To test the sensitivity of the methods to detect deviations from Gaussian profiles, a Hermite-Gaussian 1–0 mode of the same spot size[10] was evaluated. The calculated result of scanning along the x axis is

$$[P(x_s)/P_0]_{\mathrm{TEM}_{10}} = (1/2)\,\mathrm{erfc}(u) + (u/\sqrt{\pi})\exp(-u^2),$$
$$u = (\sqrt{2})(x - \bar{x}_s)/w. \tag{14}$$

The major deviation from the error function occurs at $u_M = \pm 1/\sqrt{2}$ with an amount of $\sqrt{(2\pi e)} \approx 24\%$. This suggests that the detection of admixtures of such eigenmodes with a power of less than, say, 10% of the fundamental Gaussian has to make use of other methods, e.g., of Fabry-Perot scanning in the frequency domain.

It may be noted that by using the least-squares program above, an iteration of the type given in Ref. 11 can be avoided: The program finds directly one waist to satisfy both the asymptotic slope $1/z_0 = \lambda/\pi w_0^2$ as well as the minimum w_0 of the function $w(z) = w_0\sqrt{[1 + (z - z_w)^2/z_0^2]}$ with the criterion of minimizing random errors.

This paper is an outcome of research done under AFOSR grant 84-0058.

References

1. J. A. Arnaud, W. M. Hubbard, G. D Mandeville, B de la Claviere, E. A. Franke, and J. M. Franke, "Technique for Fast Measurement of Gaussian Laser Beam Parameters," Appl Opt. 10, 2775 (1971); Y. Suzaki and A. Tachibana, "Measurement of the μm Sized Radius of Gaussian Laser Beam Using the Scanning Knife-Edge," Appl. Opt. 14, 2809 (1975); J. M Khosrofian and B. A. Garetz, "Measurement of a Gaussian Laser Beam Diameter Through the Direct Inversion of Knife-Edge Data," Appl. Opt. 22, 3406 (1983); M. Mauck, "Knife-Edge Profiling of Q-Switched Nd:YAG Laser Beam and Waist," Appl. Opt. 18, 599 (1979).
2. The required size of the detector and its distance from the edge may be estimated as follows: An aperture of a diameter 4 w passes over 99.9% of a circular Gaussian beam of spot size w As far as diffraction effects due to the edge are concerned, the power of the cylindrical waves in the shadow region diminishes as $(kz)^{-1}$ [M. Born and E. Wolf, *Principles of Optics* (Pergamon, New York, 1975), Chap. 11], which amounts to $\sim 10^{-5}$ for $\lambda = 633$ nm at $r = 1$ cm off the edge: with a detector placed more than 1 cm behind the edge we can safely disregard diffraction effects
3. M. Abramowitz and I. A. Stegun, Eds., *Handbook of Mathematical Functions* (Dover, New York, 1972), Chap. 7.
4. Ref. 3, Chap. 26. The approximation 26 2.16 therein is over 2 orders of magnitude more accurate than that used by Khosrofian and Garetz (see Ref. 1); however the following approximation, which is similar to the latter in structure is also accurate to $\pm 1 \times 10^{-5}$ for $-\infty \leqslant x \leqslant +\infty$:
   $Q(x) \simeq [1 + \exp[f(x)]]^{-1}$, $f(x) = a_1x + a_2x^3 + a_3x^5 + a_4x^7$,
   $a_1 = 1.595700$, $a_2 = 0.072953$, $a_3 = -0.000324$,
   $a_4 = -0.0000350$.
5. Error function paper is available as graph paper no. 46800 from Keuffel & Esser, covering relative magnitudes from 0 01 to 99 99, a better-suited variant of it, covering 0.15–0.85, was devised by D. Preonas, Dayton Research Institute, in 1980 This latter graph paper makes use of the central portion of the Gaussian only, thus avoiding errors due to deviations of the beam from Gaussian shape in the tails.
6. W. C. Hamilton, *Statistics in Physical Science* (Ronald Press, New York, 1964), Chaps. 4 and 5.
7. The program is available on request.
8. F. A. Jenkins and H. E. White, *Fundamentals of Optics* (McGraw-Hill, New York, 1976), Sec. 9.9.
9. Ref. 8, p. 169, Eq. (9q).
10. This situation prevails in eigenmodes of a ring laser.
11. T. D. Baxter, T. T. Saito, G. L. Shaw, R. T. Evans, and R. A. Motes, "Mode Matching for a Passive Resonant Ring Laser Gyroscope," Appl. Opt. 22, 2487 (1983).

APPENDIX C

OPTICAL RESONATOR WITH EXTERNAL SOURCE: EXCITATION OF THE HERMITE-GAUSSIAN MODES

Optical resonator with an external source: excitation of the Hermite-Gaussian modes

M. R. Sayeh, H. R. Bilger, and T. Habib

The amplitudes of excited Hermite-Gaussian modes in an astigmatic resonator due to an injected astigmatic Gaussian mode are calculated. Various types of misadjustment are considered: offset ϵ; tilt α; mismatch o. For small misadjustments the amplitudes are fast-converging series in the mismatch parameter o and in the misalignment parameter ξ. For mismatch, only even-indexed Hermite-Gaussians appear. The theory is applied to an experimental result involving a 3.15-m square ring interferometer. Formulas for power matching are derived, and control loops to eliminate all but the Gaussian mode are proposed.

I. Introduction

The ideal situation of a perfectly coupled system of a source with a passive resonator via a matching and aligning circuit is given in Fig. 1. The adjustment box has two purposes:

(a) It aligns the optical axis of the injecting laser beam with the optical axis of the resonator modes.

(b) It matches the spatial distribution of the injected beam mode with the distribution of the corresponding resonator mode. (Frequency matching [tuning] is not discussed in this paper.)

Figure 1 depicts a ring resonator as a case of an astigmatic resonator. However, we will limit the discussion to resonators where two orthogonal symmetry axes exist, one in the plane of the ring (x axis) and another perpendicular to this plane (y axis).

Unlike a self-aligning optical oscillator (laser), such a resonator has its own eigenmodes independent of the injected beam so that imperfect spatial coupling necessarily excites unwanted modes for any degree of misadjustment, be it misalignment or mismatch: unlike the self-excited laser, there is no threshold either for higher-order modes.

The purpose of adjustment is thus to effect a perfect spatial overlay mode by mode of a laser beam with the corresponding resonator modes.

This analysis attempts to quantify the effects of misadjustment. Of the many types of mode realizable, only Hermite-Gaussians are used because they are the most commonly occurring; they can be naturally extended to systems with two orthogonal planes of symmetry, as is the case in ring resonators; misadjustment can be separately discussed in each plane; conversely, the simpler case of a linear resonator can be obtained in a straightforward manner.[1]

The formalism of astigmatic Hermite-Gaussian modes (HGs) is developed in Sec. II. The expansion of a beam in the resonator's eigenmodes is formalized in Sec. III. We inject a misadjusted Gaussian beam (Sec. IV) and expand it in the resonator's modes (Sec. V). The resulting general equation is then used to predict power matching, i.e., the degree to which power is transferred from the beam to the Gaussian of the resonator (Sec. VI). Formulas for the HGs are then developed and specialized to misalignment and mismatch in Sec. VII. Finally, the analysis is applied to empirical data obtained on a square ring where misadjustment parameters are quantitatively assessed from a measured spectrum of HGs (a scan) (Sec. VIII). A summary of the results and consequences is drawn in Sec. IX.

II. Astigmatic Hermite-Gaussian Modes

HGs solve the Fresnel-Kirchhoff diffraction integral as well as the paraxial wave equation.[2] For purposes of this analysis we will discuss the electric field of a HG polarized in the $\hat{x}$ direction ($\hat{x}$ is a dimensionless unit vector), propagating in the positive z direction (the optical axis), in vacuum:

$$\mathbf{E}_{mnq}(x,y,z,t) = \sqrt{(2\eta P_{mn})}\,U_{mn}(x,y)\exp(-jkz + j\omega t)\hat{x}, \quad (1)$$

where η = vacuum impedance = $(\mu_0/\epsilon_0)^{1/2}$, P_{mn} = beam power, k = wave number, ω = angular frequency, with

$$\begin{aligned} U_{mn}(x,y) = U_m(x)U_n(y) = &\{[\sqrt{2}/(\sqrt{\pi 2^m m! w_x})]^{1/2} H_m(\sqrt{2}x/w_x) \\ &\times \exp[-j(k/2q_x)x^2 + j(m+1/2)\phi_x]\} \\ &\times \{[\sqrt{2}/(\sqrt{\pi 2^n n! w_y})]^{1/2} H_n(\sqrt{2}y/w_y) \\ &\times \exp[-j(k/2q_y)y^2 + j(n+1/2)\phi_y]\}. \end{aligned} \quad (2)$$

The authors are with Oklahoma State University, School of Electrical & Computer Engineering, Stillwater, Oklahoma 74078.

Received 17 June 1985.
0003-6935/85/223756-06$02.00/0.

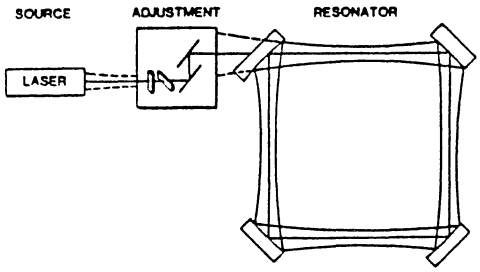

Fig. 1. Laser source coupled into a resonator via an adjustment circuit. The function of the latter is to align and match the source to the (astigmatic) resonator.

Fig. 2. Misaligned system: The laser's optical axis z' is offset by ϵ and tilted by α against the resonator's optical axis z. In this figure the waists of laser and resonator are at the same z and equal in size.

This is the astigmatic formulation of the lateral field distribution, where w_x, w_y are the spot sizes in the x and y directions, respectively (the spots are generally elliptical), H_m and H_n are Hermite polynomials of degree m and n, respectively, q_x and q_y are the complex curvature parameters, and ϕ_x and ϕ_y are phases.

The Hermite-Gaussian function $U_{mn}(x,y)$ is thus completely separated into a product of two functions, each depending only on one lateral variable. Since all operations below preserve this independence, we will treat one variable only: $\mu = m$ or n, $\nu = x$ or y. We have then $H_\mu(\nu)$, with $H_0(\nu) = 1, H_1(\nu) = 2\nu, H_2(\nu) = 4\nu^2 - 2$, etc, and

$$q_\nu^{-1} = R_\nu^{-1} - j2/kw_\nu^2 \ (R_\nu = \text{curvature radius}). \tag{3}$$

The fields E_{mnq} are normalized so that

$$1/2 \int_{-\infty}^{+\infty} \int_{-\infty}^{+\infty} (E_{mnq}^* E_{mnq}/\eta) dx dy = P_{mn}, \tag{4}$$

i.e., P_{mn} is the power of the mnq mode. The HG functions are normalized so that

$$\int_{-\infty}^{+\infty} |U_\mu(\nu)|^2 d\nu = 1.$$

Useful approximations for phase ϕ_ν, spot size w_ν and curvature radius R_ν:

All modes have the same dependence of z. For the phase,

$$\phi_\nu(z) = \tan^{-1}[(z - z_{0\nu})/z_{R\nu}], \tag{5}$$

where the argument of $\tan^{-1}$ is the distance from the waist site $z_{0\nu}$ in terms of the Rayleigh range $z_{R\nu}$. In a system which is not far from adjustment, we can assume that all waists are well within the Rayleigh ranges of each other, and we may approximate $\phi_\nu \simeq 0$. For the curvature radii, we have

$$R_\nu(z) = (z - z_{0\nu})[1 + z_{R\nu}^2/(z - z_{0\nu})^2]. \tag{6}$$

Again we may occasionally put $R_\nu \to \infty$ close to the waist sites, in which case $q_\nu(z)$ becomes purely imaginary, $q_\nu \to jkw_{0\nu}^2/2$. Finally the spot sizes are

$$w_\nu^2(z) = w_{0\nu}^2[1 + (z - z_{0\nu})^2/z_{R\nu}^2] \tag{7}$$

and may be approximated by their respective waist sizes $w_{0\nu}$.

III. Expansion of an Injected Beam into the Resonator's Eigenmodes

The functions U_{mn} form an orthogonal and complete set.[3] We, therefore, expand the x component of the field $\mathbf{E}_L$ of an injected beam in terms of this set, i.e.,

$$E_L = \sum_{m=0}^{\infty} \sum_{n=0}^{\infty} A_{mn} E_{mnq} \ (E_L = x \text{ component of injected field}) \tag{8}$$

with dimensionless but generally complex expansion coefficients A_{mn}. The fields E_{mnq} are given by Eq. (1), where $P_{mn} = P_L$ (power of the injecting beam). We have

$$\sum_{m=0}^{\infty} \sum_{n=0}^{\infty} |A_{mn}|^2 = \sum_{m=0}^{\infty} |A_m|^2 \sum_{n=0}^{\infty} |A_n|^2 = 1, \tag{9}$$

$$A_\mu = \int_{-\infty}^{+\infty} U_\mu^*(\nu) U_L(\nu) d\nu, \tag{10}$$

where $U_\mu^*(\nu)$ is the conjugate-complex of the μth eigenmode, and $U_L(\nu)$ is the HG function of the injected E field.

IV. Injection with Misadjusted Gaussian Beam

In the following we use an injected astigmatic Gaussian beam ($m = n = 0$) with spot sizes w_{Lx} and w_{Ly}. Its optical axis shall be parallel-shifted against the resonator's z axis by ϵ_x and ϵ_y in the x and y directions, respectively. It shall also be tilted by angles α_x and α_y off the resonator's z axis (see Fig. 2). Finally we allow the waist sites of injected beam and resonator modes to be different as well as the waist sizes (see Fig. 3).

The integrals [Eq. (10)] are evaluated in the coordinate system of the resonator: x = in-plane coordinate of resonator; y = perpendicular to plane; z = optical axis of ring, forming a right-handed coordinate system, origin at waist location.

In the tilted and offset coordinate system $x'y'z'$ of the injected beam, the field distribution is

$$\begin{aligned} \mathbf{E}_L(x',y',z',t) = {} & \sqrt{(2\eta P_L)(2/\pi w_{Lx} w_{Ly})^{1/2}} \\ & \times \exp[-j(k/2)(x'^2/q_{Lx} + y'^2/q_{Ly})] \\ & \times \exp(-jkz' + j\omega t)\hat{x}'. \end{aligned} \tag{11}$$

This results from Eqs. (1) and (2) with $\mu = 0, \phi_\nu = 0$.

Expressing the primed coordinates in the unprimed coordinates of the resonator system, we have

$$x' = (x - \epsilon_x)\cos\alpha_x - z\sin\alpha_x \simeq x - \alpha_x z - \epsilon_x,$$
$$y' = (x - \epsilon_x)\sin\alpha_x \sin\alpha_y + (y - \epsilon_y)\cos\alpha_y - z\cos\alpha_x \sin\alpha_y \simeq y - \alpha_y z - \epsilon_y, \quad (12)$$
$$z' = (x - \epsilon_x)\sin\alpha_x \cos\alpha_y + (y - \epsilon_y)\sin\alpha_y + z\cos\alpha_x \cos\alpha_y \simeq z + \alpha_x x + \alpha_y y,$$

retaining only terms of first order in the misalignment parameters ϵ_x, ϵ_y, α_x, α_y.

The pivot point is assumed to be at $z = 0$. For small deviations from $z = 0$, the errors are of second order in the parameters.

Furthermore, $\hat{x}' = \hat{x}\cos\alpha_x - \hat{z}\sin\alpha_x \simeq \hat{x}$ is set. The $\hat{z}$ component is eliminated because it is orthogonal to $\hat{x}$.

The field of the injected beam is, therefore, approximately $\mathbf{E}_L(x,y,z,t) = (2\eta P_L)^{1/2} U_L(x,y) \exp(-jkz + j\omega t)\hat{x}$, with

$$U_L(\nu) = [\sqrt{2}/(\sqrt{\pi} w_{L\nu})]^{1/2} \times \exp[-j(k/2q_{L\nu})[\nu^2 - 2(\epsilon_\nu - q_{L\nu}\alpha_\nu)\nu + \epsilon_\nu^2]] \quad (13)$$

V. Expansion of Injected Field in the Resonator Eigenmodes

Equations (2), (10), and (13) are used in a physical situation where the waist sites in the two planes are well within the respective Rayleigh ranges of each other, so that we can put $\phi_x = \phi_y \simeq 0$ and also $jkw_\nu^2/2 \simeq q_\nu \simeq -q_\nu^*$. Equation (13) yields

$$A_\mu = \int_{-\infty}^{+\infty} U_\mu^*(\nu) U_L(\nu) d\nu.$$

It is convenient to introduce a misalignment parameter ξ and a mismatch parameter o, namely,

$$\xi_\nu = (\epsilon_\nu - q_{L\nu}\alpha_\nu)/w_\nu, \qquad o_\nu = [(q_\nu^* + q_{L\nu})/(q_\nu^* - q_{L\nu})]^{1/2}, \quad (14)$$

where the offset is measured in units of the spot size, the tilt in units of beam divergence, and the mismatch in terms of the ratio of the complex curvatures. Note that for perfect adjustment, $\xi_\nu = o_\nu = 0$. For coinciding waist sites, the mismatch parameter o can be written as $o_\nu = [(w_\nu^2/w_{L\nu}^2 - 1)/(w_\nu^2/w_{L\nu}^2 + 1)]^{1/2}$, i.e., in terms of the waist sizes directly. The amplitudes are then evaluated from the integral (10)[4]. The result can be written in the form

$$A_\mu = W_\nu \times \Xi_\nu \times M_{\mu\nu},$$

with

$$W_\nu = [(w_\nu/w_{L\nu})2q_{L\nu}/(q_{L\nu} + q_\nu)]^{1/2} = (1 - o_\nu^4)^{1/4},$$
$$\Xi_\nu = \exp[-q_\nu\epsilon_\nu^2/q_{L\nu}w_\nu^2 + \xi_\nu^2(q_\nu/q_{L\nu})q_\nu/(q_\nu + q_{L\nu})] = \exp[-(q_\nu/q_{L\nu})[\epsilon_\nu^2/w_\nu^2 - (1 + o_\nu^2)\xi_\nu^2/2]], \quad (15)$$
$$M_{\mu\nu} = (2^\mu\mu!)^{-1/2} o_\nu^\mu H_\mu[\xi_\nu(1 + o_\nu^2)/\sqrt{2}o_\nu].$$

This rather cumbersome equation gives the response of the resonator to a misadjusted Gaussian input beam. It is not easily exploited. The factor $M_{\mu\nu}$, which governs the convergence of the series, does not generally converge monotonically (see Sec. VIII). It is, however, normalized in the sense that $M_{0\nu} = 1$. Also the requirement that $A_0 = 1$, $A_\mu = 0$ for perfect adjustment is satisfied.

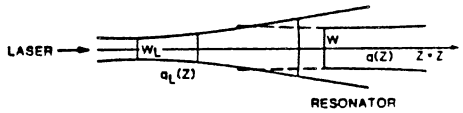

Fig. 3. Mismatched system: Laser and resonator have different waist sizes located at different z values. The system is aligned, however, i.e., $z = z'$

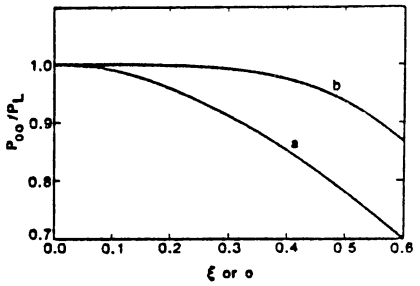

Fig. 4. Power transfer from the Gaussian laser beam to the Gaussian of the resonator in a misadjusted system: a, power transfer ratio in a misaligned system, where $\xi = (|\xi_x|^2 + |\xi_y|^2)^{1/2}$ is set. For $\xi \to 0$, $P_{00}/P_L \to 1$, asymptotically; b, power transfer in a mismatched system, where $o = o_x = o_y$ is set. Again there is asymptotic convergence for $o \to 0$.

VI. Power Transfer into the Resonator's Gaussian

This problem is of obvious interest for the design of such a system.

For the resonator Gaussian, $A_{00} = W_x W_y \Xi_x \Xi_y$. For perfect adjustment, $\xi_\nu = 0$, $q_\nu = q_{L\nu}$ (for both $\nu = x$ and $\nu = y$), $o_\nu = 0$, $A_{00} = 1$, and the power transfer is $P_{00}/P_L = |A_{00}|^2 = 1$.

In the special case of proper alignment (but mismatch), Eq. (15) produces with $\Xi_\nu = 1$ the simple result

$$P_{00}/P_L = |W_x|^2 |W_y|^2 = (|1 - o_x^4||1 - o_y^4|)^{1/2} (\epsilon_\nu = \alpha_\nu = 0, o \neq 0). \quad (16)$$

The upper curve in Fig. 4 shows the power transfer vs o, where $o_x = o_y = o$. As Eq. (16) suggests the transfer is not very sensitive to small mismatch. For example, if the spot sizes of resonator and laser are 10% different, we obtain $P_{00}/P_L = 0.991$, i.e., <1% of the power is put into HGs. In the special case of proper match (but misalignment), we have, with $q_\nu = q_{L\nu}$, $W_\nu = 1$:

$$P_{00}/P_L = |\Xi_x|^2 |\Xi_y|^2 = \exp[-(\epsilon_x^2/w_x^2 + k^2 w_x^2 \alpha_x^2/2^2)] \times \exp[-(\epsilon_y^2/w_y^2 + k^2 w_y^2 \alpha_y^2/2^2)], = \exp[-(|\xi_x|^2 + |\xi_y|^2)] \quad (o = 0, \xi_\nu \neq 0) \quad (17)$$

displayed as the lower curve in Fig. 4, where $\xi^2 = |\xi_x|^2 +$

$|\xi_y|$ is set. Equation (17) shows again that offset and tilt are in quadrature. In a system with 10% misalignment ($\xi^2 = 0.1^2 = 0.01$), ~1% of the power is lost.

VII. Size of the Hermite-Gaussians in a Misadjusted System

To find the amplitudes of HGs ($m \neq 0, n \neq 0$), it is convenient to avoid factors which do not depend on m or n. We form

$$A_\mu/A_0 = M_{\mu\nu} = (o_\nu^\mu/2^{\mu/2}\sqrt{\mu!})H_\mu[\xi_\nu(1 + o_\nu^2)/\sqrt{2}o_\nu], \quad (18)$$

with the two special cases

$$A_\mu/A_0 = \xi_\nu^\mu/\sqrt{\mu!} \sim (2\pi\mu)^{-1/4}(e\xi_\nu^2/\mu)^{\mu/2} (match, o_\nu \to 0), \quad (19)$$

$$A_{2\mu}/A_0 = [(-1/2)^\mu\sqrt{(2\mu)!}/\mu!]o_\nu^{2\mu} \sim (-o_\nu^2)^\mu/(\pi\mu)^{1/4}, \quad (20)$$

$$A_{2\mu+1}/A_0 = 0 \text{ (alignment, } \xi_\nu \to 0).$$

Equations (19) are obtained using $H_\mu(\nu \to \infty) \sim (2\nu)^\mu$ and Stirling's approximation for the factorial. Eqs. (20) by using $H_\mu(\nu \to o) \simeq (-1)^{\mu/2}\mu!/(\mu/2)!$ for even μ and $H_\mu(\nu \to o) \simeq 0$ for odd μ.

The asymptotic forms are given to demonstrate the fast convergence of the mode amplitudes, once near adjustment with $|\xi_\nu| \ll 1$, and $|o_\nu| \ll 1$ is achieved. They are, by the way, within 4% of the explicit forms for $\mu \geq 2$. Equations (20) also show that pure mismatch produces even-indexed HGs only, as opposed to pure misalignment. That odd-indexed HGs vanish in an aligned system follows directly from a consideration of the symmetry of an aligned beam with respect to both the x and y direction. Figure 5 show the isophotes of an offset beam which is also mismatched in the y direction but matched in the x direction. If the offset is removed, the lower part of the figure has the odd-indexed modes absent. Figure 6 gives a plot of the field vs x of an injected beam with the sizable offset $\xi_x = 1$, i.e., $\epsilon_x = w_x$. Note that the amplitude A_5 has already drastically decayed ($A_5/A_0 \simeq 0.09$); the power in the 5–0 mode is <1% of the power of the Gaussian mode.

As far as the phases are concerned, we note that, o_ν being either real or purely imaginary for a nearly matched system, the HGs for the aligned system [Eq. (20)] have either the same phase ($w_L > w$) or alternating signatures ($w_L < w$); for a misaligned system [Eq. (19)], the phases depend on the relative contribution of tilt and offset.

VIII. Application to Misadjusted Resonator System

In a ring interferometer the beam path encloses a finite area, and the modes are astigmatic. The injecting laser, therefore, needs to be matched in the x and y planes besides having to be aligned in both coordinates.

The identification of the modes in such an astigmatic cavity is done by evaluating the eigenfrequencies of the resonator. From Ref. 5 it follows that

$$f_{mnq} = (c/L)[(m + 1/2)\beta_x/2\pi + (n + 1/2)\beta_y/2\pi] + (c/L)q, \quad (21)$$

where the angles β_x and β_y depend on geometry and

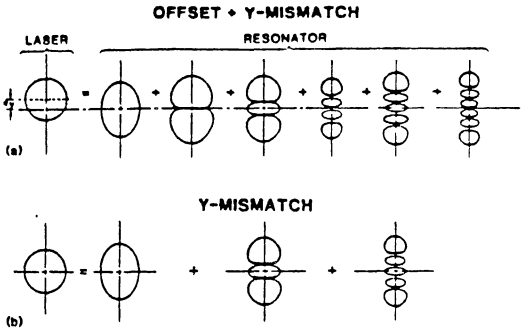

Fig. 5. Isophotes of laser beam and resonator modes with proper adjustment in the x direction (a) Offset ϵ_ν and mismatch o_ν produce all $E_{o,n,q}$ modes in the resonator. (b) Mismatch alone produces only even-indexed Hermite-Gaussian modes. Since the system is perfectly adjusted in the x direction, all excited Hermite-Gaussians have $m = 0$.

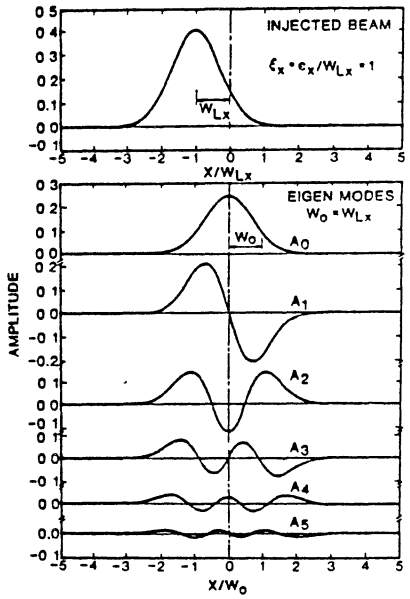

Fig. 6. Field distribution vs normalized x axis due to an offset beam with misalignment parameter $\xi_x = 1 + j0$ (pure offset, $\epsilon_x = w_{Lx}$). Shown is the incoming beam and the first five excited eigenmodes. All vertical scales are equal.

mirror curvature radii R. We analyzed a square ring[6] of perimeter $L = 3.15$ m, with two diagonally placed spherical mirrors of equal curvature radius $R = 6.00$ m. The other two mirrors are flat. The beam is injected at one of the flat mirrors. The frequency differences are

$$f_{mnq} - f_{00q} = (c/\pi L)[m \cos^{-1}(1 - L/\sqrt{2}R) + n \cos^{-1}(1 - L/2\sqrt{2}R)] \quad (22)$$

Fig. 7. Fabry-Perot scan of a misadjusted system. The two Gaussian modes 0,0,q and 0,0,q + 1 are prominent because the injected Gaussian beam is not far from adjustment. The identification of the peaks in the free spectral range of the resonator is

1	0,11,q-2	7	0,8,q-1	overlapping are	1 2,3,q-1 (?)
2	0,6,q-1	8	0,3,q	the following	4 2,4,q-1
3	0,1,q	9	0,9,q-1	modes:	7 2,0,q
4	0,12,q-2	10	0,4,q		9 2,1,q (?)
5	0,7,q-1	11	0,10,q-1		11 2,2,q.
6	0,2,q	12	0,5,q;		

The system has the two mismatch parameters $o_x = 0.53 - j0.66$, $o_y = 0.40 - j0.76$, and the two misalignment parameters $\xi_x = = 0 + j0$ and $\xi_y = 0.255 - j0.153$; the latter corresponds to an offset of 180 μm and a tilt angle of 49 sec of arc. The lower sequence are least-squares fitted amplitudes. The fit of the 0-n sequence has residuals of 2.4% average.

as shown in Fig. 7. In the free spectral range between the Gaussian 0,0,q and 0,0,q + 1 modes (q is unknown), seventeen modes are identified including 0,n,q, modes (n = 0–12) and 2,n,q modes (n = 0–4).

The analysis proceeds as follows: The absence of the 1,n,q modes suggests alignment in the plane of the ring [Eq. (20)], $\epsilon_x = \alpha_x = 0$. The relatively large ratio of the 0,0,q modes to others suggests a near-adjusted situation, i.e., ϵ_y and α_y are small. The mismatch is known from the optical circuit: $o_x = 0.53 - j0.66$ $o_y = 0.40 - j0.76$. Thus we expect even-indexed modes to appear in both planes, i.e., m = 2,4,6, . . . , as well as n = 2,4,6 . . . .

The general Eq. (18) has to be applied for the y direction, whereas Eq. (20) is applicable to the HGs in the x direction. The unknown parameter is ξ_y.

In a least-squares fit, the nine largest measured ratios of the 0–n peaks to the 0–0 peak were fitted with the squared absolute value $|A_\mu/A_0|^2$ from Eq. (18) using the adjustable parameter ξ_y. The fit produced rms residuals of 2.4% (with respect to the 0–0 peak) with $|\xi_y| = 0.30$, and $\epsilon_y = 180\ \mu$m, $\alpha_y = 49$ arc-sec. These are plausible values, considering that even nuances of the spectrum were verified as, for example, the rank of almost every 0–n peak. although the series was not monotonic.

Of the five 2–n peaks, only the 2–0 peak is prominent. Nevertheless, Eq. (20) predicts these five peaks to within a factor of 2 assuming that the nearly coinciding 0–n lines have negligible powers. Figure 8 depicts the same system but with an improvement in the matching circuitry: A spherical lens had been put in a compromise position to effect a better match with the result $o_x = 0 + j0.328$, $o_y = 0.303 + j0$, ($|o_y| \simeq |o_x|$).

These values for mismatch are already quite low, although an effort has not yet been made in this experiment to inject an astigmatic beam. The calculated power transfer into the 0–0 mode is [Eq. (16)] $P_{oo}/P_L = 0.990$; i.e., only 1% of the power is lost.

Concurrently, a much better alignment has been achieved. The emergence of the 1–0 mode as well as the 0–1 mode signifies, however, that there is now misalignment in both planes. The estimates from these two small peaks are $|\xi_x| \sim 0.16$ and $|\xi_y| \simeq 0.19$. The paucity of the data does not allow determination of a real and imaginary part of ξ, i.e., of ϵ and α in Fig. 8. Further experiments to relate the Hermite-Gaussian mode structure to misadjustment are quite welcome.

IX. Discussion and Conclusion

The calculations presented in this paper allow a quantitative estimate of power matching as well as the prediction of the HG structure in a resonator excited by a misadjustment beam. The two complex parameters ξ (misalignment) and o (mismatch) have been introduced to account for offset, tilt, and mismatch. In an astigmatic system, a separate set of parameters is necessary for each of the two orthogonal planes.

The analysis of data obtained on the example, a square ring with a perimeter of 3.15 m available in the literature, demonstrates that quite detailed information can be obtained about the degree of adjustment of a system through this theory.

Such knowledge may be put to good use in the engineering of a precision instrument as, e.g., a large ring interferometer. The necessary precision of adjustment can be calculated through a consideration of the effects of misadjustment on the desired data.

The loss of power in the desired 0–0 mode is an obvious effect. It is itself Gaussian in the two parameters offset and tilt, whereby these parameters, which are in quadrature, are naturally measured with respect to spot size and beam divergence. For a mismatched beam the loss is proportional to o^4, meaning that power

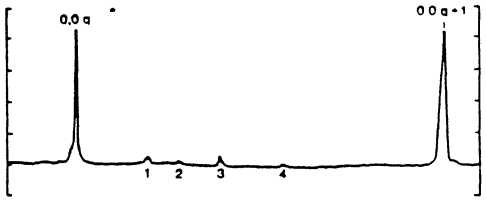

Fig. 8. Fabry-Perot scan of a better adjusted system (compare with Fig. 7). Both mismatch and misalignment are improved, the former by inserting a (spherical) lens in a compromise position. Identification of peaks: 1, 0,1,q; 2, 1,0,q; 3, 0,2,q; 4, 2,0,q. There is now misalignment and mismatch in both directions, although reduced. The parameters are (compare with Fig. 7) $o_x = 0 + j0.33$, $o_y = 0.30 + j0$; $|\xi_x| \simeq 0.16$, $|\xi_y| \simeq 0.19$. The near symmetry of o_x and o_y signifies that $q_L/q_y \sim q_x/q_L$; i.e., the mismatch has been properly distributed to the two directions.

loss becomes relatively harmless once $|\beta| \ll 1$ and $|\alpha| \ll 1$, near adjustment, is achieved.

Another effect to be considered is frequency pulling. If we define it as the difference δf between the frequency f_0 of a Gaussian with amplitude A_0 and the frequency of the composite peak due to the presence of a HG with frequency f_1 and amplitude A_1, we get for this kind of pulling $\delta f/f_0 = (A_1/A_0)(1/2Q)^4/(f_1/f_0 - 1)^3$, where $Q = f_0/\Delta f$ is the quality factor of the resonator. On the basis that δf ought to be less than a given value, A_1/A_0 can be estimated and the degree of necessary adjustment predicted.

The ambiguity of the ring's output due to the presence of several modes is to be considered as a sort of noise and again can be suppressed with proper adjustment techniques.

Finally we propose a control scheme for adjustment of the system injection resonator. It makes use of the orthogonality and symmetry of the modes with respect to specific misadjustments:

(1) Pick up the 0–1 mode from a scanner and control with it vertical alignment. Since offset and tilt are in quadrature, each type of misalignment can be adjusted separately.

(2) Use the 1–0 mode to control the horizontal alignment in a similar way.

Note that in particular any mismatch does not affect the amplitude of these two modes.

(3) Once these modes disappear, any residual 0–2 and 2–0 modes are then due to mismatch. Although we do not believe that a once-matched system goes into significant mismatch due to ambient effects, there is nevertheless the possibility of using these latter modes to control the match by using zoom systems with cylindrical lenses in the respective planes.

This work has been done under Air Force grant AFOSR 84-0058.

References

1. Several aspects of coupling and power conversion between modes have already been discussed by H. Kogelnik, "Coupling and Conversion Coefficients for Optical Modes," in *Proceedings, Symposium on Quasi-Optics, June 1964*, J. Fox, Ed. (Polytechnic Press, Brooklyn, N.Y., 1964), p. 333.
2. H. A. Haus, *Waves and Fields in Optoelectronics* (Prentice-Hall, Englewood Cliffs, N.J., 1984), Chap. 4.
3. A. E. Siegman, "Orthogonality Properties of Optical Resonator Eigenmodes," Opt. Commun. 31, 369 (1979).
4. I. S. Gradshteyn and I. M. Ryzhik, *Table of Integrals, Series, and Products* (Academic, New York, 1980). With the substitution $x = \sqrt{2}r/w_r$, integral Eq. (10) is transformed in an integral of the type 7.374, No. 10, p. 838.
5. S. A. Collins, "Analysis of Optical Resonators Involving Focusing Elements," Appl. Opt. 3, 1263 (1964).
6. T. D. Baxter, T. T. Saito, G. L. Shaw, R. T. Evans, and R. A. Motes, "Mode Matching for a Passive Resonant Ring Laser Gyroscope," Appl. Opt. 22, 2487 (1983).

APPENDIX D

LIST OF EQUIPMENT USED IN EXPERIMENTS

DESCRIPTION	MANUFACTURER	MODEL AND TYPE
Laser	Coherent	200; Freq.-Stabilized
Beam Aligner	Oriel	6550; Angle & Trnsltns.
Spectrum Analyzer	Coherent	240-2-B
Mirror-holders	-	- ; angle adjustments
Granite Block	Collins	MicroFlat; 9'x6'x8"
Mirrors	-	1 cm spot diameter
Matching lens	-	f = 0.78 cm
Iris	-	1 mm - 1 cm aperture
Laser mounts	Oriel	Adjustable lens mounts
Output detector	UDT	555-D (hybrid)
Voltmeter	Keathly	610 Electrometer
Oscilloscope	Tektronix	547
Computer	Texas Instrmts.	TIPC
A/D conv. I.C.	National Semic.	ADC 0804

VITA

Taufiq Habib

Candidate for the Degree of

Master of Science

Thesis: EXPERIMENTAL CONSTRUCTION AND ANALYSIS OF A PASSIVE LASER RING RESONATOR

Major Field: Electrical Engineering

Biographical:

Personal: Born in Karachi, Pakistan on March 17, 1959

Education: Received the Bachelor of Science degree from N.E.D University in Karachi, with a major in Electronics Engineering in 1983; completed requirements for the Master of Science Degree at Oklahoma State University in December, 1986.

Professional Experience: Graduate Research and Teaching Assistant at Oklahoma State University from February 1984 to May 1986.

Papers Co-Authored: 1) "Knife-edge scanning of an astigmatic Gaussian beam" 2) "Optical resonator with external source: excitation of the Hermite-Gaussian modes" 3) contributed to AFOSR report on "Modeling a Large Ring Resonator Gyroscope".